Holocene history of the 79° N ice shelf reconstructed from epishelf lake and uplifted glaciomarine sediments

James A. Smith[1], **Louise Callard**[2], **Michael J. Bentley**[3], **Stewart S. R. Jamieson**[3], **Maria Luisa Sánchez-Montes**[4], **Timothy P. Lane**[5], **Jeremy M. Lloyd**[3], **Erin L. McClymont**[3], **Christopher M. Darvill**[6], **Brice R. Rea**[7], **Colm O'Cofaigh**[3], **Pauline Gulliver**[8], **Werner Ehrmann**[9], **Richard S. Jones**[10], and **David H. Roberts**[3]

[1]British Antarctic Survey, High Cross, Madingley Road, Cambridge, CB3 0ET, UK
[2]School of Geography, Politics and Sociology, Newcastle University, Newcastle upon Tyne, NE1 7RU, UK
[3]Department of Geography, Durham University, Durham, DH1 3LE, UK
[4]INSTAAR – Institute of Arctic and Alpine Research, University of Colorado Boulder, Boulder, CO 80309-0450, USA
[5]School of Biological and Environmental Sciences, Liverpool John Moores University, Liverpool, L3 3AF, UK
[6]Department of Geography, University of Manchester, Manchester, M13 9PL, UK
[7]School of Geosciences, University of Aberdeen, Aberdeen, AB24 3TU, UK
[8]NERC Radiocarbon Facility, East Kilbride, G75 0QF, UK
[9]Institute for Geophysics and Geology, University of Leipzig, Leipzig 04103, Germany
[10]School of Earth Atmosphere and Environment, Monash University, Clayton, Victoria, Australia

Correspondence: James A. Smith (jaas@bas.ac.uk)

Abstract. Nioghalvfjerdsbrae, or 79° N Glacier, is the largest marine-terminating glacier draining the Northeast Greenland Ice Stream (NEGIS). In recent years, its ~ 70 km long fringing ice shelf (hereafter referred to as the 79° N ice shelf) has thinned, and a number of small calving events highlight its sensitivity to climate warming. With the continued retreat of the 79° N ice shelf and the potential for accelerated discharge from NEGIS, which drains 16 % of the Greenland Ice Sheet (GrIS), it has become increasingly important to understand the long-term history of the ice shelf in order to put the recent changes into perspective and to judge their long-term significance. Here, we reconstruct the Holocene dynamics of the 79° N ice shelf by combining radiocarbon dating of marine molluscs from isostatically uplifted glaciomarine sediments with a multi-proxy investigation of two sediment cores recovered from Blåsø, a large epishelf lake 2–13 km from the current grounding line of 79° N Glacier. Our reconstructions suggest that the ice shelf retreated between 8.5 and 4.4 ka cal BP, which is consistent with previous work charting grounding line and ice shelf retreat to the coast as well as open marine conditions in Nioghalvfjerdsbrae. Ice shelf retreat followed a period of enhanced atmospheric and ocean warming in the Early Holocene. Based on our detailed sedimentological, microfaunal, and biomarker evidence, the ice shelf reformed at Blåsø after 4.4 ka cal BP, reaching a thickness similar to present by 4.0 ka cal BP. Reformation of the ice shelf coincides with decreasing atmospheric temperatures, the increased dominance of Polar Water, a reduction in Atlantic Water, and (near-)perennial sea-ice cover on the adjacent continental shelf. Along with available climate archives, our data indicate that the 79° N ice shelf is susceptible to collapse at mean atmospheric and ocean temperatures ~ 2 °C warmer than present, which could be achieved by the middle of this century under some emission scenarios. Finally, the presence of "marine" markers in the uppermost part of the Blåsø sediment cores could record modern ice shelf thinning, although the significance and precise timing of these changes requires further work.

1 Introduction

The Greenland Ice Sheet (GrIS) is losing mass at an accelerating rate and is currently the largest single contributor to global sea-level rise (Oppenheimer et al., 2019). Model projections suggest that mass loss will continue to accelerate in a warming climate, with the potential for ~ 7.4 m of sea-level rise (Morlighem et al., 2017; Aschwanden et al., 2019). Mass loss has been driven by increases in atmospheric temperature (Fettweis et al., 2017; Hanna et al., 2021) and ocean (Straneo and Heimbach, 2013; Wood et al., 2021) warming, which have resulted in enhanced melting of both the ice sheet surface and the undersides of marine-terminating glaciers respectively. Despite an improved understanding of the drivers of recent mass loss, the short time span of the observational record provides a limited time series with which to understand the complex, and often non-linear, response of the margins of the GrIS to climate forcing (Nick et al., 2010). This restricts our ability to reliably forecast how ice sheets will evolve in the future (Seroussi et al., 2013). In this context, reconstructions of past ice sheet responses to atmospheric and ocean-driven forcing can be used to validate and test the sensitivity of predictive models. In turn, this can lead to a better understanding of the feedbacks that amplify or dampen mass loss and whether tipping points exist, beyond which retreat is irreversible (Aschwanden et al., 2019).

The 79° N Glacier is the largest of three marine-terminating glaciers of the Northeast Greenland Ice Stream (NEGIS; Fig. 1) and contains enough ice to raise the global sea level by 0.57 m (An et al., 2021). Until recently, 79° N Glacier was assumed to be relatively stable (Joughin et al., 2010), but recent observations indicate increasing surface velocities and glacier thinning (Khan et al., 2014; Mayer et al., 2018; An et al., 2021). Mass loss has occurred as several small calving events at the ice shelf margin, equating to a ~ 4 % reduction in the total area of the ice shelf between 1999 and 2013 (Blau et al., 2021). During approximately the same period (1998–2016), the ice shelf has lost one-third of its thickness in the region of the Midgårdsormen Ridge (Mayer et al., 2018), ~ 5 km downstream of the grounding line (Fig. 1). These changes are thought to have been driven by both atmospheric and ocean warming. The circulation of relatively warm Atlantic Water beneath the ice shelf (Schaffer et al., 2020), which likely penetrates all the way to the grounding line (Bentley et al., 2022), is driving basal melt rates of ~ 10 m yr^{-1}. Average air temperatures have also increased by ~ 3 °C during the past 40 years (Turton et al., 2021), with supraglacial melt lakes now a persistent feature (Leeson et al., 2015; Hochreuther et al., 2021). Given that further retreat is predicted following the break-up of Spalte Glacier (a northern tributary of the 79° N ice shelf; Fig. 1) in 2019 and 2020, which could activate further dynamical thinning and acceleration of the NEGIS drainage basin (Khan et al., 2014; Choi et al., 2017), it has become increasingly important to understand the long-term dynamics of the ice shelf in order to contextualise the recent changes.

Based on ^{10}Be surface exposure ages, the deglaciation of Nioghalvfjerdsfjorden occurred between 9.2 and 7.9 ka (Larsen et al., 2018). This concurs with earlier work dating whale bones and other macrofossils along the margins of the 79° N ice shelf, which indicated that it retreated inboard of the current location during the Holocene Thermal Maximum (HTM; ~ 8.0–5.0 ka cal BP) (Bennike and Weidick, 2001), when atmospheric temperatures were elevated above present. Ocean warming and reduced sea ice have also been documented to the east of 79° N in the Early Holocene (Werner et al., 2016; Syring et al., 2020; Pados-Dibattista et al., 2022), suggesting that ice shelf retreat was driven by both atmospheric and ocean forcing. In this paper, we utilise chronologically constrained lacustrine sediment cores recovered from the northern margin of the ice shelf and combine these with new and existing (Bennike and Weidick, 2001; Larsen et al., 2018) age control from uplifted glaciomarine deposits to provide a detailed Holocene history of the 79° N ice shelf. We discuss these results in the context of both atmospheric and oceanic warming, which in the past forced ice shelf retreat, and use this to contextualise changes due to ongoing climate warming.

2 Study area and approach

Blåsø is a large epishelf lake located at sea level on the northern margin of 79° N Glacier (Fig. 2). It is located within the East Greenland Caledonides, a series of W-directed thrust sheets displaced against the rocks of the Palaeoproterozoic–Mesoproterozoic foreland (Higgins and Kalsbeek, 2004). The crystalline basement, consisting of strongly deformed Archaean and Palaeoproterozoic granitoid rocks, is overlain by Mesoproterozoic–Neoproterozoic and lower-Palaeozoic strata. To the east of Blåsø, outcrops of quartzite/sandstones (Hovgaard Ø Formation), dolerites, and flood basalts (Midsommersø Dolerite Formation) are exposed. Moving westwards, these are overlain by the Neoproterozoic Rivieradal Group, consisting of conglomerate, sandstone turbidite, and mudstone units (Smith et al., 2004a). In turn, these are overlain by the limestones, mudstones, and dolomites of the Odin Fjord, Turesø, and Børglum River formations further west (Smith et al., 2004b). The n-shaped lake abuts the ice shelf at two locations, approximately 2 and 13 km from the grounding line of 79° N Glacier. Blåsø has a well-resolved tidal signal and is stratified. At its eastern end, where the deepest water has been documented (Bentley et al., 2022), a 145 m thick layer of fresh to brackish water overlies a warm (< 0.7 °C) marine layer, sourced from modified Atlantic Water which flows beneath the ice shelf and into and out of the lake driven by the local tides. The halocline at 145 m acts as a proxy for the draught of the floating tongue of 79° N at the eastern margin, assuming the ice is in hydrostatic equilibrium (Bentley
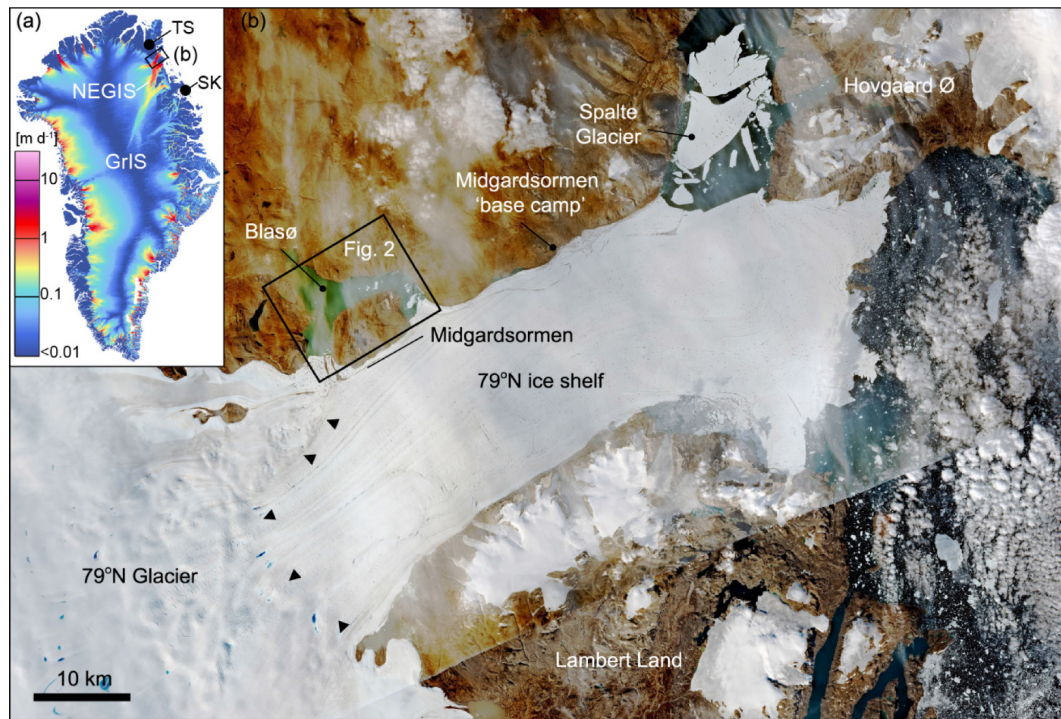
Figure 1. (a) Ice velocity map of the Greenland Ice Sheet (GrIS) (Mottram et al., 2019), showing the location of the Northeast Greenland Ice Stream (NEGIS), the study area presented in panel **(b)**, Trifna Sø (TS), and Store Koldewey/Duck Lake (SK). **(b)** Sentinel-2 L2A imagery of 79° N Glacier and its floating ice shelf (contains modified Copernicus Sentinel data, August, 2020, processed by the Sentinel Hub EO Browser; https://www.sentinel-hub.com/, last access: 14 November 2022). Blåsø is located 2–13 km from the grounding line (GL) of 79° N Glacier, delineated by black triangles. The remnants of Spalte Glacier, a northern tributary of 79° N Glacier which broke up in 2020, is also shown.

et al., 2022). While marine water is only detected at the eastern margin, there is observational evidence (e.g. sub-ice-shelf fish species observed in the lake) to suggest that the western margin periodically connects to the sub-shelf cavity, allowing small volumes of marine water to mix into the western part of the lake (Bentley et al., 2022). The present-day limnology of Blåsø, and therefore its concomitant sedimentary signature, is controlled by the 79° N ice shelf "dam", without which the lake would become a marine embayment (see Fig. 10 in Smith et al., 2006). The sedimentary records deposited within epishelf lakes can, therefore, provide continuous archives of past ice shelf dynamics (Smith et al., 2006). For example, epishelf lakes in Antarctica and the Canadian Arctic have yielded detailed ice shelf histories, including information on the timing of ice shelf collapse and reformation, as well as elucidating the drivers of change from biological and geochemical proxies contained within the lake sediments (Bentley et al., 2005; Smith et al., 2007; Antoniades et al., 2011). Proximal to Blåsø, uplifted glaciomarine sediments around the lake can be found up to 40 m a.s.l (metres above sea level) (Bennike and Weidick, 2001). These sediments were linked to a period of ice shelf absence during the Early Holocene, but they have not been analysed in detail nor related to the adjacent epishelf lake sediments. By investigating the lacustrine and uplifted marine sediments in combination, a detailed history of the 79° N ice shelf is reconstructed.

3 Methods

3.1 Core recovery and sampling of uplifted glaciomarine sediments

Fieldwork was carried out between 19 July and 11 August 2017 when, with the exception of the far eastern end of the lake which abuts the 79° N ice shelf, Blåsø was largely ice-free. Following a detailed bathymetric survey (Bentley et al., 2022), coring was focused within a ~ 90–100 m deep central basin (Fig. 2) where sub-bottom profiler data showed stratified sediments up to ~ 20 m in thickness (Fig. 3). Core sites LC7 (79.589° N, 22.494° E; 87 m water depth) and LC12 (79.594° N, 22.4423° E; 90 m water depth) targeted the thinner drape at the edge of the basin infill (Fig. 3) to ensure that the longest (temporal) record was recovered. An additional advantage of coring the central basin is that it is currently isolated from marine water, as the ice shelf draft – in its current configuration – is sufficient to block marine water from filling the entire basin (Bentley et al., 2022). Detec-
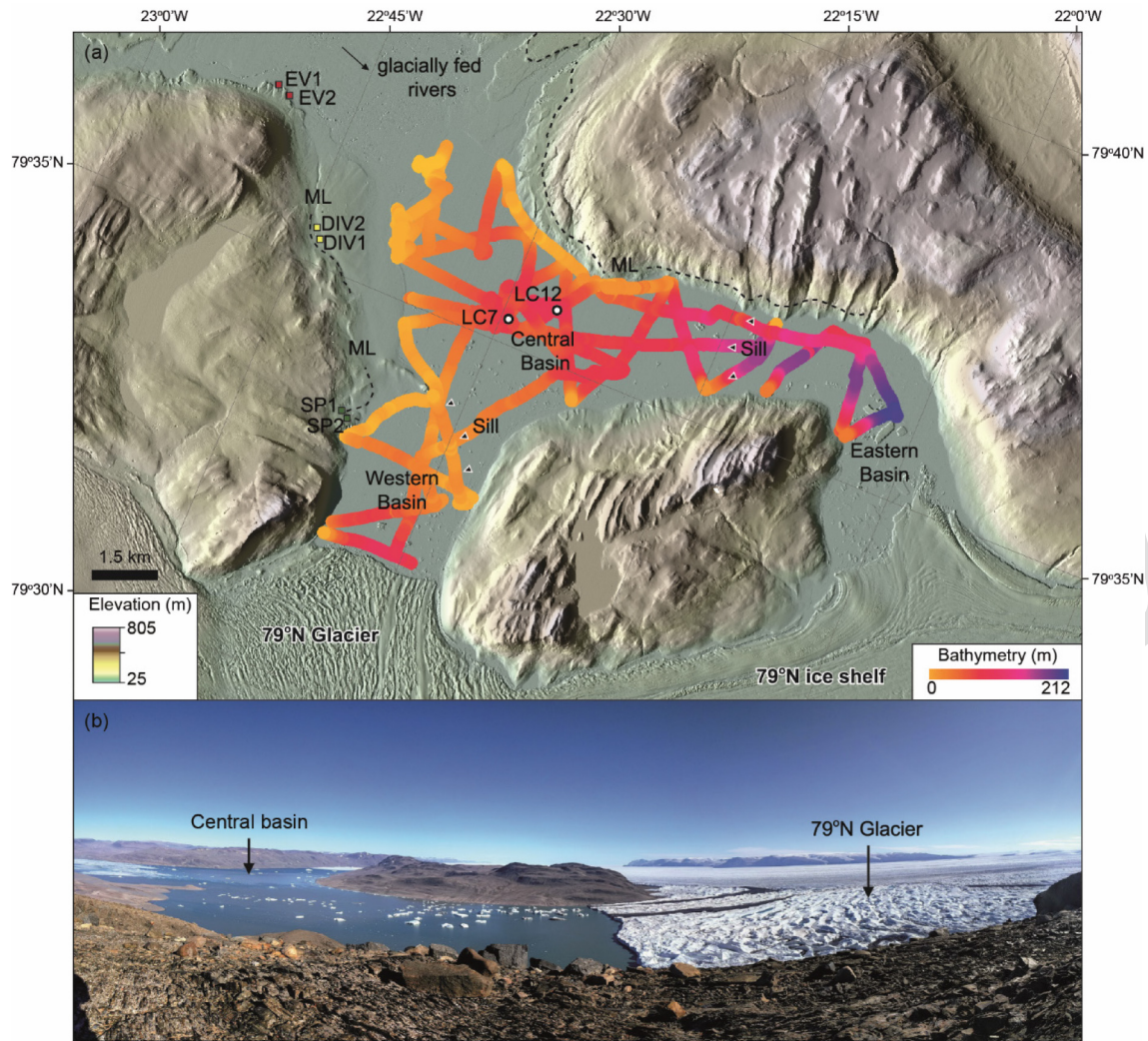
Figure 2. (a) Bathymetry of Blåsø, showing the locations of sediment cores LC7 and LC12 as well as the western, central, and eastern basins. The bathymetry is overlain by ArcticDEM imagery (Porter et al., 2018). The central basin is currently isolated from marine water by shallow sills (black triangles) at the margins of the western and eastern basins. Also shown are the locations of uplifted glaciomarine sediments (SP1–SP2, DIV1–DIV2, and EV1–EV2) and the location of glacially fed rivers entering the basin. Dashed black lines delineate the marine limit (ML). Panel **(b)** presents a photograph (taken by David H. Roberts) of Blåsø looking east. The 79° N Glacier is shown in the foreground (right of frame) along with the approximate location of the central basin.

tion of marine markers in the sedimentary record at this site would present clear evidence of a significantly thinner than present or entirely absent ice shelf. Furthermore, the central basin is sufficiently distal from the glacially fed rivers enter-
ing the northwestern side of the lake, thereby avoiding excessive coarse-sediment inputs (observed during fieldwork) which could overprint the palaeoenvironmental record.

Overlapping 2 m long sediment cores were recovered with a UWITEC KOL "Kolbenlot" percussion piston corer to a
total sediment depth of 3.74 m (LC7) and 5.24 m (LC12). Coring was performed from a UWITEC raft, fitted with a 15-horsepower Yamaha outboard motor. Multi-proxy analyses (detailed below) were performed on both cores, with a

particular focus on "marine" lithofacies (LF1) identified in LC7 and LC12. Additional analyses (e.g. clay mineral and biomarkers) were performed on LC12 because it recovered the longer sequence and was, therefore, prioritised as the "master core".

Uplifted glaciomarine sediments were described following standard sedimentological procedures (Evans and Benn, 2004). In situ mollusc (*Hiatella arctica*) and gastropod samples were recovered from the uplifted glaciomarine sediment at various locations above the western shore of Blåsø, from sea level up to 40 m a.s.l. (Fig. 2). Only articulated shells were collected and dated. The altitude was measured using handheld GPS units. Uplifted glaciomarine sediments and
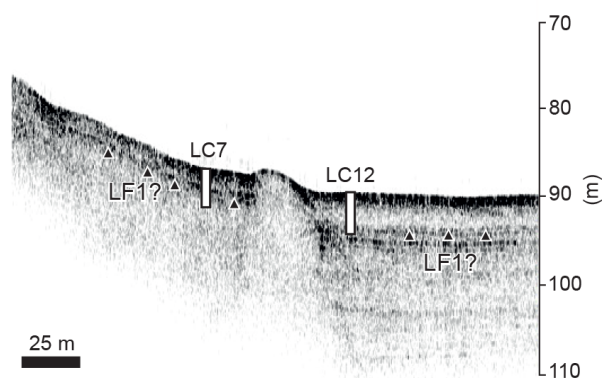
Figure 3. Sub-bottom profile across coring sites LC7 and LC12 in the central basin of Blåsø. The prominent reflector ∼ 3–4 m below the lake floor (black triangles) is likely related to the deposition of lithofacies (LF) 1 during ice shelf retreat.

push ridges were also surveyed using a theodolite from base (lake) level. Foraminifera are also present in the uplifted marine sediment but were only assessed qualitatively.

3.2 Sedimentological properties, physical properties, and geochemical analyses

Physical properties (e.g. magnetic susceptibility and wet bulk density) and X-radiographs were measured on the whole core using a Geotek multi-sensor core logger (MSCL) and Geotek X-ray CT core imaging system (MSCL-XCT) respectively (at the Department of Geography, Durham University) to characterise lithological properties and infer the depositional environment(s). Core sections were then split, described, and subsampled. Next, 1 cm thick sediment slices were taken every 10–20 cm. Grain-size analysis was performed on core LC12 using a Beckman Coulter LS 13 320 laser diffraction particle size analyser. Prior to analysis, sediment samples were treated with 20 % hydrogen peroxide to digest the organic material. Once the organic material had been digested, the sample was centrifuged, and a solution of 20 mL of distilled water and 2 mL of 35 % sodium hexametaphosphate was added to disaggregate the sample. High-resolution elemental abundances were measured on the split core using a Geotek X-ray fluorescence (MSCL-XRF) instrument at 1 mm resolution. We use elemental ratios of Ti/Ca as a proxy for terrigenous source variations (i.e. siliciclastic vs. carbonate rocks), while Mn/Fe and Br concentrations provide semi-quantitative information about lake oxygenation (Naeher et al., 2013) and marine organic carbon content (Ziegler et al., 2008) respectively. Ti contents in marine sediments are directly linked to the terrigenous (siliciclastic) sediment supply delivered by fluvial and/or aeolian transport processes (Arz et al., 1999; Nace et al., 2014), while Ca concentrations reflect changes in the production of calcium carbonate ($CaCO_3$) by marine plankton (Bahr et al.,

2005). High Ti/Ca ratios are indicative of increased terrigenous flux. The behaviour of Fe and Mn is strongly dependent on the processes of oxidation and reduction. Reducing conditions are the result of O_2 consumption during organic matter (OM) remineralisation, which releases Fe and Mn. Because Fe oxidises faster than Mn, high Mn accumulation and, thus, high (low) Mn/Fe ratios reflect oxic (anoxic) conditions. Bromine (Br) is used as a proxy for marine organic carbon, as bromine is found at higher concentrations in marine, compared with terrestrial, organic matter (Ziegler et al., 2008; Seki et al., 2019). Finally, an aliquot of the ≤ 2 μm fraction was used to determine the relative concentrations of the clay minerals smectite, illite, chlorite, and kaolinite in LC12 using an automated powder diffractometer system (Rigaku MiniFlex) with Co$K\alpha$ radiation (30 kV, 15 mA) at the Institute for Geophysics and Geology (University of Leipzig, Germany). The clay mineral identification and quantification followed standard X-ray diffraction methods (Ehrmann et al., 2011), and this information is used to reconstruct sediment provenance and pathways. Illite and chlorite are detrital clay minerals which are typically derived from the physical weathering of crystalline (granitoids and low-grade chlorite-bearing metamorphic rocks) and basement rocks (basic rocks, dolerites), respectively. Smectite normally reflects volcanic sources (i.e. basalts and volcanic glass), whilst kaolinite is a product of chemical weathering, characteristic of moist, temperate to tropical regions. Kaolinite generally indicates the presence of older sedimentary strata (i.e. mudstones/shales).

3.3 Foraminiferal analysis

A total of 16 (LC12) and 6 (LC7) samples were processed for foraminiferal analysis to reconstruct the environmental conditions in Blåsø. The sample volume varied between 0.5 and 5 mL (cm^3) depending on the average foraminiferal concentration (estimated based on the initial scanning of samples). The variation in sample size was designed to allow ∼ 300 to 500 specimens to be counted from all samples. Once extracted, samples were soaked in deionised water for several hours to help disaggregate the sediment. Samples were then washed through a 500 and 63 μm mesh sieve to concentrate the foraminifera. The material collected on the 63 μm mesh sieve was retained for foraminiferal analysis. Foraminifera were identified and counted from the wet (non-buffered) residue under a binocular microscope.

3.4 Lipid biomarker extraction and analyses

A total of 22 sediment samples from LC12 were prepared for lipid biomarker analyses. Lipids were microwave-extracted from 0.4 to 2 g of freeze-dried and homogenised sediment using dichloromethane : methanol (3 : 1) at an oven temperature of 70 °C for 2 min, following Kornilova and Rosell-Mele (2003). Internal standards of known concentration

Table 1. Summary of the lipid biomarker proxies analysed.

Fraction	Equations	Interpretation	References
Ketone	$U_{37}^{K} = \frac{[C_{37:2}]-[C_{37:4}]}{[C_{37:2}]+[C_{37:3}]+[C_{37:4}]}$	Surface water temperature and salinity	Prahl and Wakeham (1987)
Ketone	$\%C_{37:4} = \frac{[C_{37:4}]}{[C_{37:2}]+[C_{37:3}]+[C_{37:4}]} \cdot 100$	Surface water temperature and salinity	Bendle and Rosell-Melé (2004)
Ketone	$K_{37}/K_{38} = \frac{\sum[C_{37}]}{\sum[C_{38}]}$	Changes in Haptophyceae species producing alkenones	Prahl et al. (1988)
Ketone	$U_{37}^{K} = \frac{SWT - 31.8}{40.8}$, $r^2 = 0.96$, and $n = 34$	Freshwater surface water temperature calibration	D'Andrea et al. (2011)
Ketone	$U_{37}^{K} = 0.082 SWT - 0.63$	Marine surface water temperature calibration	Bendle and Rosell-Melé (2004)
Ketone	$APE = \frac{mass\ 2\text{-}nonadecanone}{[2\text{-}nonadecanone]} \cdot [C_{37}A]$	Haptophyceae productivity export	Prahl et al. (1988); Rosell-Melé and McClymont (2007)
n-Alkane	Terrigenous OM $= [C_{27}] + [C_{29}] + [C_{31}]$	Terrigenous organic matter from higher plants	Rieley et al. (1991)
n-Alkane	Aquatic OM $= [C_{15}] + [C_{17}] + [C_{19}]$	Aquatic productivity export of bacteria and phytoplankton	Cranwell (1973)
n-Alkane	$CPI = \frac{\frac{[C_{25-33}(odd)]}{[C_{24-32}(even)]} + \frac{[C_{25-33}(odd)]}{[C_{26-34}(even)]}}{2}$	Sediment maturity	Bray and Evans (1961)
n-Alkane	Pristane/phytane $= \frac{[pristane]}{[phytane]}$	Relative oxidative or reductive conditions, sediment maturity	Ten Haven et al. (1988); Bray and Evans (1961)
n-Alkane	$C_{31}/C_{29} = \frac{[C_{31}]}{[C_{29}]}$	Relative grassy or woody vegetation contribution	Guillemot et al. (2017)
n-Alkane	$TAR = \frac{[C27]+[C29]+[C31]}{[C15]+[C17]+[C19]}$	Relative terrestrial and aquatic contributions	Cranwell (1973)

(5α-cholestane, heptatriacontane, and 2-nonadecanone) were added to aid quantification. The extracted sediment was centrifuged at 2500 rpm for 5 min. The solvent was decanted and then taken to near dryness with a stream of N$_2$. The total lipid extract was separated into three fractions using glass Pasteur pipettes packed with extracted cotton wool and a 4 cm silica column (high-purity grade, pore size 60 Å, 220–440 mesh particle size, 35–75 μm particle size; Sigma-Aldrich) for flash chromatography. Sequential elution with hexane, dichloromethane, and methanol (four columns each) yielded n-alkane, ketone, and polar fractions respectively.

Biomarkers were quantified and identified using gas chromatography with flame ionisation (GC-FID) and mass spectrometry (GC-MS), as outlined in detail in Sánchez-Montes et al. (2020). The internal standards were used to calculate lipid mass, normalised to the original extracted dry weight of sediment. We employ a range of n-alkanes and ketones as environmental proxies, utilising a series of equations used to determine the relative contribution of bacteria and phytoplankton to sediments, as well as indicators of water temperature and salinity (Table 1). The terrigenous and aquatic OM equations in Table 1 were normalised to the weight of the sediment extracted. Moreover, because Blåsø has experienced both marine (LF1) and lacustrine (LF2–LF3) conditions, the alkenone U_{37}^{K} index was converted into surface water temperature (SWT) using both the surface temperature calibration equation of D'Andrea et al. (2011), which was developed for lakes in West Greenland, and the marine tem-

perature calibration in Bendle and Rosell-Mele (2004), developed for the Nordic Seas (Table 1).

3.5 Core chronology

The chronology for LC7 and LC12 was established using accelerator mass spectrometry (AMS) radiocarbon (^{14}C) dating. Where possible, calcareous microfossils (mixed benthic foraminifera) were dated, and bulk (acid-insoluble organic matter – AIOM) sediment was only dated in the absence of microfossils. Moreover, to assess the reliability of the AIOM fraction, we performed "paired" foraminifera and AIOM dating on two horizons (~ 297 and 327 cm). Cores were also inspected for other datable macrofossils (mosses, algae, and shells) but were found to be barren. The ^{14}C dating of samples from the lake cores and of macrofossils (molluscs and gastropods) from the raised marine deposits was undertaken at the NERC Radiocarbon Laboratory (Environment) in East Kilbride, UK (denoted using the prefix "SUERC-"); the Keck-CCAMS facility, University of California, Irvine, USA (denoted using the prefix "UCIAMS-"); and Beta Analytic, Miami, USA (denoted using the prefix "BETA-"). Radiocarbon ages were calibrated to calendar years before present (cal yr BP, where present is 1950 CE) using the calibration software CALIB 8.1.0 (Stuiver and Reimer, 1993), the Marine20 calibration curve (Heaton et al., 2020), and a ΔR of 0 ± 0 years, following Hansen et al. (2022). Marine20 estimates an increase in the (globally aver-
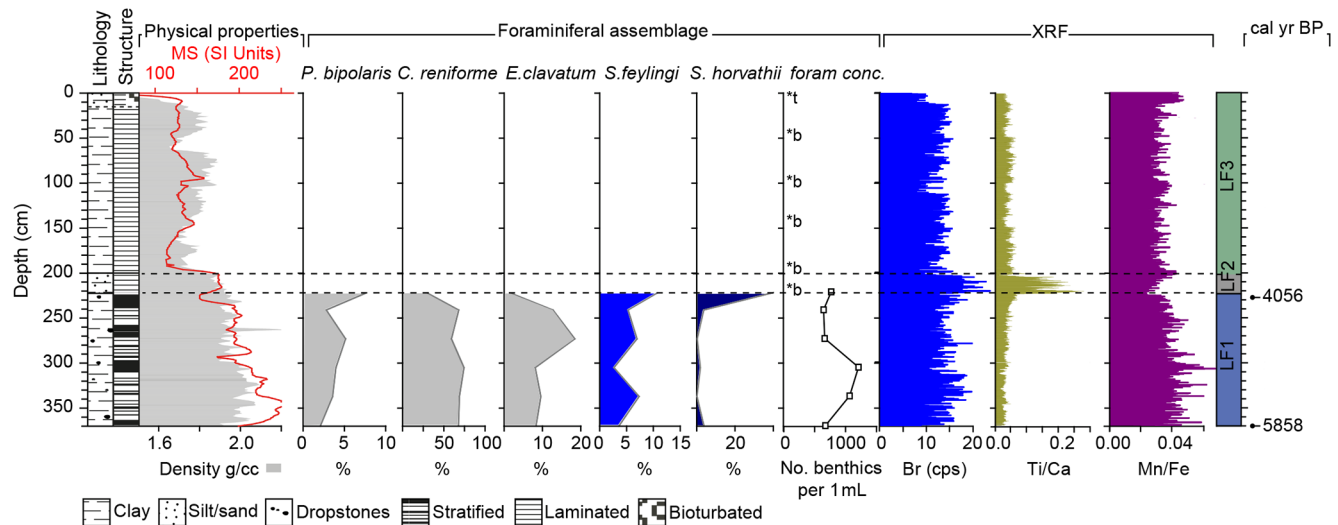
Figure 4. Multi-proxy data for core LC7, including simplified core lithology/structure, physical properties (magnetic susceptibility (MS) and density), foraminiferal assemblage data (barren (b) and trace (t; < 20) foraminifera), and selected XRF-scanner data. Horizontal (dashed) lines delineate the main lithofacies (LF) 1–3. Calibrated ages are shown on the right panel.

aged) marine reservoir age compared with Marine13, ranging from ∼ 550–410 ^{14}C yr for the pre-bomb period. This is ∼ 150 years older than the marine reservoir age in Marine13, which was 405 ^{14}C years (Reimer et al., 2013). Thus, a ΔR of 0 ± 0 years, as advocated by Hansen et al. (2022), essentially replicates previously published work from the region using Marine13, e.g. ΔR 150 ± 0 years (Larsen et al., 2018), and results in near-identical calibrated ages. A ΔR of 0 ± 0 years is also very similar to the geographically nearest data point to 79° N in the Marine20 marine reservoir database (map no. 31 shows a ΔR of 3 ± 60 years; Funder, 1982). However, as outlined in O'Regan et al. (2021), the absence of a priori information regarding local marine reservoir corrections for many areas of Greenland could result in a broad envelope of uncertainty in calibrated ages. Unfortunately, without additional work, including the use of independent dating techniques, i.e. relative palaeointensity, it remains difficult to fully quantify this. For example, variations in sea-ice cover, different water masses, or input of glacial meltwater all have the potential to impact the local marine reservoir age (see O'Regan et al., 2021; Pados-Dibattista et al., 2022; Hansen et al., 2022; and Heaton et al., 2022, for further discussion).

4 Results and interpretation

4.1 Blåsø

LC7 consists of two overlapping ∼ 2 m long cores with a composite core recovery of 3.74 m. LC12 consists of three 2 m cores, although we only have confidence that the upper two drives overlap. The uncertain splice likely reflects movement of the raft during coring operations, with the third drive of the piston corer penetrating a different part of the sediment drape. For this reason, we only present data for the upper two sections of LC12. Multi-proxy analyses reveal three main lithofacies (LF1–LF3) in LC12 and LC7 (Figs. 4, 5).

CE1 In LF1, the lowermost sediments in both cores are generally brown, massive (LC12) to crudely stratified (LC7) clay/silts with occasional gravel- and pebble-sized clasts (Fig. 6). Magnetic susceptibility increases to a peak at ∼ 300 cm in LC12 before decreasing, and it decreases upcore in LC7 (Figs. 4, 5). LC12 shows an interval of increased coarse silt between 320 and 300 cm (Fig. 5). The clay mineral assemblage in LC12 is dominated by chlorite and illite with lower smectite and kaolinite contents (Fig. 7). XRF-scanning data show a high degree of variability throughout both cores. LF1 is characterised by low Ti/Ca (0.01–0.05) and Mn/Fe values between 0.01 and 0.05. Br values are typically high (∼ 20 cps, counts per second) but decrease between ∼ 320 and 305 cm in LC12.

Benthic foraminifera are present throughout LF1 (370.5–282 cm) in LC12 (Fig. 5) with the exception of one horizon at 314 cm, which was entirely barren. The assemblage is dominated by *Cassidulina reniforme* (> 50 %). *Elphidium clavatum* (10 %–20 %), *Stainforthia feylingi* (5 %–10 %), and *Stetsonia horvathi* (variable but up to 15 % below 300 cm) are also common. There is a significant shift in fauna in the uppermost part of LF1 (290.5–282 cm): *S. horvathi* becomes dominant (30 to > 50 %) while *C. reniforme* decreases but is still very common (20 %–30 %). The abundance of *E. clavatum* decreases to below 10 %, whereas *S. feylingi* abundance increases slightly to > 10 %. This section is also characterised by a significant increase in the foraminiferal concentration, with the uppermost sample (282 cm) having
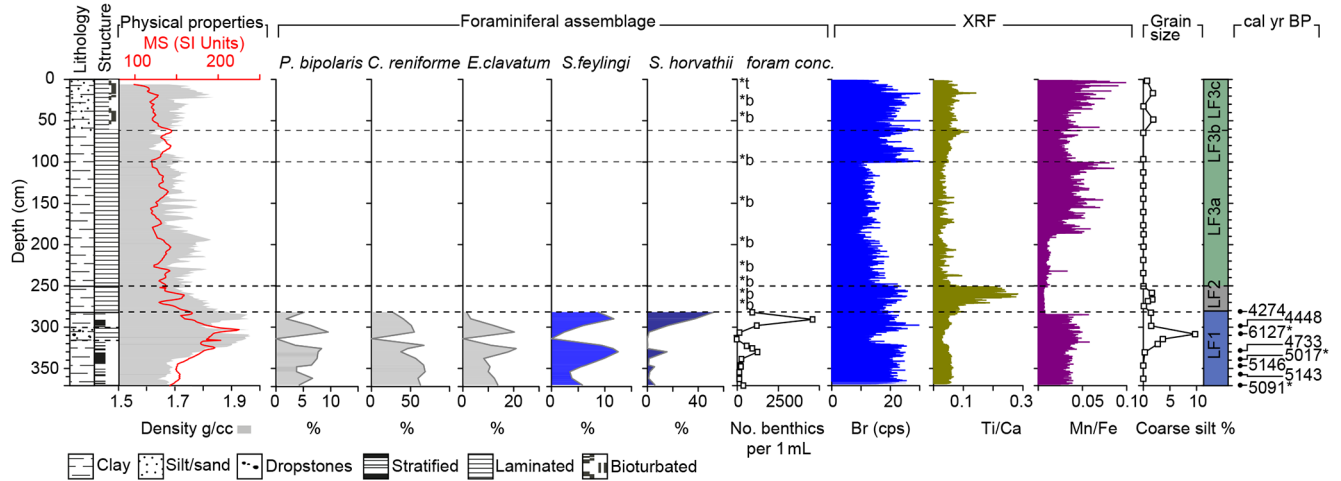
Figure 5. Multi-proxy data for core LC12, including simplified core lithology/structure, physical properties (magnetic susceptibility (MS) and density), foraminiferal assemblage data (barren (b) and trace (t; < 20) foraminifera), and selected XRF-scanner and grain-size (coarse-silt) data. Horizontal (dashed) lines delineate the main lithofacies (LF) 1–3. Calibrated ages are also shown. "*" denotes age reversals.
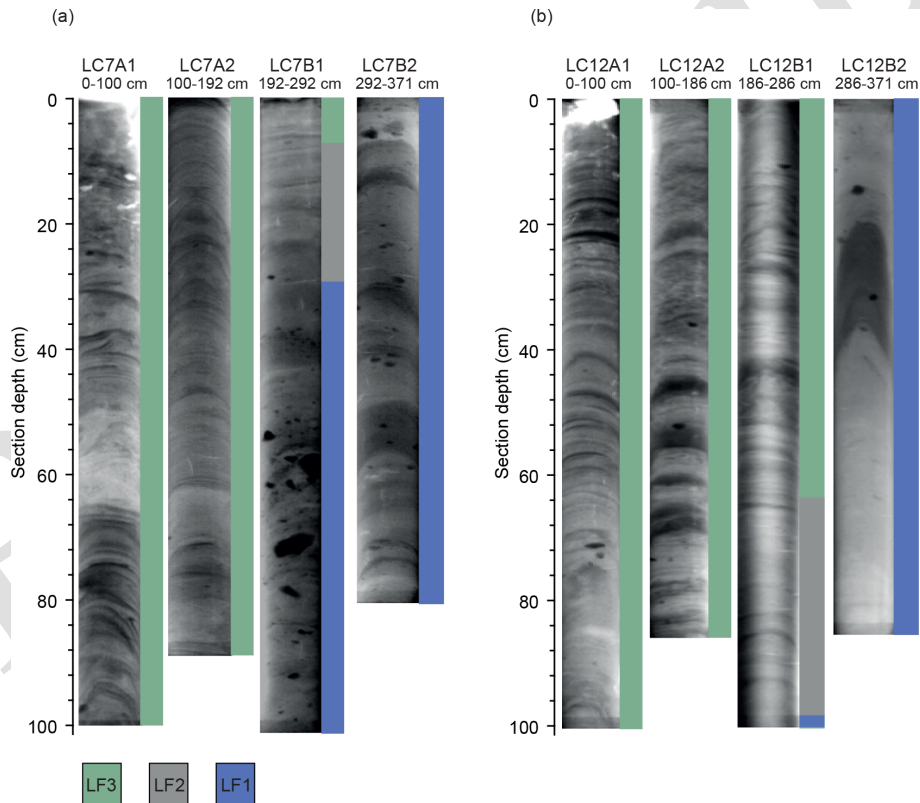
Figure 6. X-radiographs of **(a)** LC7 and **(b)** LC12 along with the associated lithofacies (LF) 1–3.

the highest foraminifera concentration per millilitre due to an increase in *S. horvathi*.

The faunal record from LC7 is very similar to LC12 (Fig. 4), although fewer samples were analysed. In total six samples were counted from 377 to 228 cm. Foraminifera disappear abruptly above 228 cm (LF1–LF2

boundary). The lower section (377–248 cm) is dominated by *C. reniforme* (60 %–75 %), with *E. clavatum* (10 %–20 %), *S. feylingi* (< 10 %), and *S. horvathi* (< 5 %) also common in decreasing importance. In the uppermost sample containing foraminifera (228 cm), the abundance of *S. horvathi* increases to > 50 %, *S. feylingi* remains common (approxi-
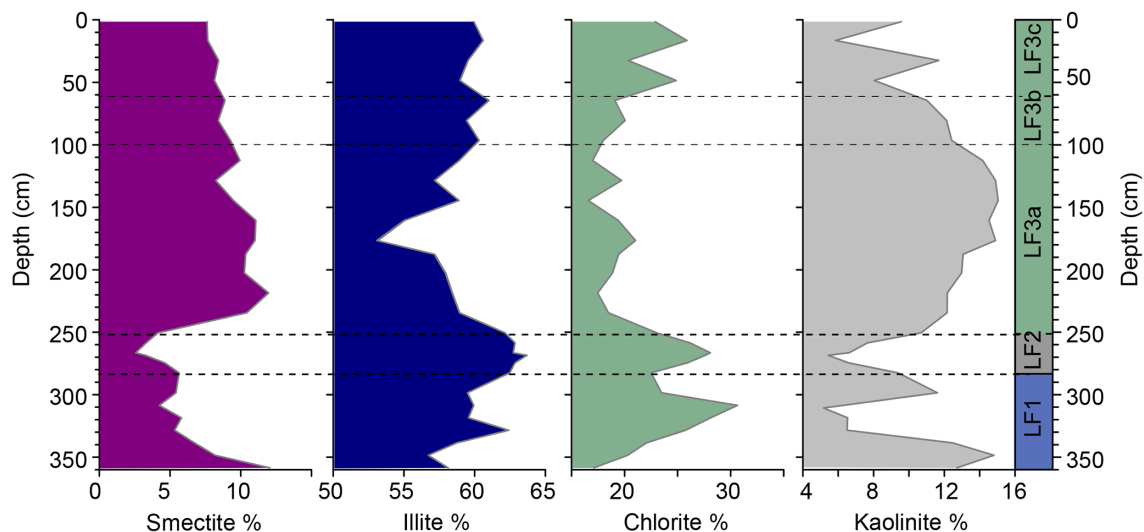
Figure 7. Clay mineral data for LC12. Horizontal (dashed) lines delineate the main lithofacies (LF) 1–3.

mately 10 %), *C. reniforme* decreases to 27 %, and *E. clavatum* decreases to < 5 %.

The U_{37}^K typically displays high values (−0.1–0.1), with a minor decrease (−0.2) at 320 cm before increasing again (Fig. 8). The %$C_{37:4}$ mirrors the U_{37}^K, with low concentrations (11 %–21 %) and a peak of 25 % at 320 cm. The K_{37}/K_{38} index is variable (0.6–1.1), with a prominent peak (1.7–2.0) between 314 and 320 cm. The terrigenous (0.07–0.1 µg g^{-1}) and aquatic OM are typically low; the latter decreases up to 320 cm (from 0.5 to 0.2 µg g^{-1}) and remains low for the rest of LF1. The terrestrial-to-aquatic ratio (TAR) and C_{31}/C_{29} are variable but show a general increasing trend. The pristane/phytane and the carbon preference index (CPI) ratios display low values (1.2–1.8 and 0.7–1.0 respectively).

With respect to the palaeoenvironmental interpretation of LF1, on the basis of abundant benthic foraminifera, high U_{37}^K, and low %$C_{37:4}$, indicative of a relatively cool and saline water column (Bendle and Rosell-Mele, 2004), this lithofacies is interpreted to have been deposited in a seasonally open marine setting. Specifically, the %$C_{37:4}$ values (10 %–25 %) indicate the absence, or low concentrations (< 30 %), of sea ice (Wang et al., 2021) and salinities similar to the North Atlantic close to the winter sea-ice edge (Wang et al., 2021). A corollary of this is that 79° N – the ice dam that currently prevents marine water from reaching the central basin of Blåsø – must have been absent at the time of deposition. The foraminiferal assemblage in the lowermost parts of LC12 and LC7 is dominated by *C. reniforme* (> 50 %), which is indicative of cold water, typical of distal glaciomarine conditions (Hald and Korsun, 1997; Slubowska et al., 2005; Slubowska-Wodengen et al., 2007; Perner et al., 2011; Consolaro et al., 2018). *E. clavatum* is also common (10 %–20 %) and has been associated with proximal to distal glaciomarine conditions (Slubowska-Wodengen et al., 2007; Perner et al., 2011;

Jennings et al., 2011). In contrast, the key Atlantic indicator species *Cassidulina neoteretis* (Jennings et al., 2011, 2004; Perner et al., 2015; Cage et al., 2021) occurs in low numbers with < 5 % abundance. Thus, the lowermost assemblage in LF1 indicates cold glaciomarine conditions with minimal evidence of Atlantic-sourced waters. Above ∼ 290 cm in LC12 and above ∼ 228 cm in LC7, cold-water indicators still dominate, but there is a significant increase in the abundance of *S. horvathi*. This species is commonly found in association with perennial sea-ice cover (Wollenburg and Mackensen, 1998) and, in some instances, below ice shelves (Jennings et al., 2020). Therefore, the dominance of *S. horvathi* suggests an increase in ice cover. An abrupt shift in alkenone producers between 300 and 314 cm (K_{37}/K_{38}) and a decrease in aquatic productivity (aquatic OM) below 300 cm also suggest a change in surface water properties (Fig. 8). Furthermore, peaks in the K_{37}/K_{38} index occur with higher %$C_{37:4}$ more closely compared to fresher North Pacific, rather than North Atlantic, waters suggesting increased sea-ice concentration (Wang et al., 2021) and/or surface Polar Water influence (Bendle and Rosell-Mele, 2004) while still allowing aquatic algae productivity. CE2 The upper and lower foraminiferal assemblages in LC12 are separated by an increase in coarse silt, with corresponding peaks in magnetic susceptibility, chlorite, and K_{37}/K_{38} (Figs. 5, 7, 8). This coarse-silt interval reflects either a period of enhanced deposition of ice-rafted debris (IRD) within an ice-free marine embayment or the first sign of glacial advance associated with ice shelf reformation. Generally, IRD-sized material (> 125 µm) is relatively rare throughout both cores; this is probably related to the bathymetry of Blåsø – specifically the ridges at both sides of the central basin (Fig. 2) which act to block large bergs from reaching the core sites. Nevertheless, coincident with the increase in coarser detri-
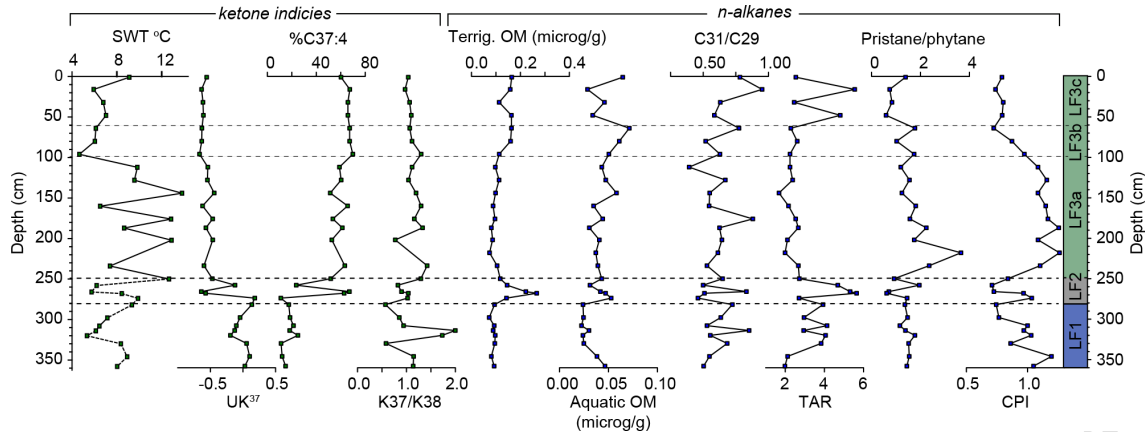
Figure 8. Biomarker (*n*-alkanes and ketone indices) data for LC12. Horizontal (dashed) lines delineate the main lithofacies (LF) 1–3. Surface water temperature (SWT) was calculated using data from both D'Andrea et al. (2011) (LF3 – solid line) and Bendle and Rosell-Mele (2004) (LF1 and LF2 – dashed line) for the "lake" and "marine" phases respectively.

tus in LC12, we see a minor shift to colder/less-saline water ($< U_{37}^K$; $> \%C_{37:4}$) (Prahl and Wakeham, 1987; Bendle and Rosell-Mele, 2004). We envisage that, as the ice shelf started to ground at the eastern and western mouths of Blåsø, marine water was periodically restricted as fresher (lacustrine) conditions became more prevalent. Clay mineral data reveal information about sediment pathways linked to catchment geology. The Blåsø area comprises the northern part of the East Greenland Caledonides, and the bedrock is primarily composed of crystalline basement except for a few places on Lambert Land and north of Nioghalvfjerdsfjorden where Palaeoproterozoic–Mesoproterozoic sediments and basalts are present (Smith et al., 2004a). While high concentrations of illite likely reflect local input from the Rivieradal Group (Neoproterozoic sandstones/siliciclastic sediments primarily composed of quartz and feldspar grains as well as small amounts of mica) and the limestone-bearing Odins Fjord Formation, the elevated chlorite content could reflect one of two sources, both of which require the absence of the 79° N ice shelf: (1) input from the basaltic rocks of Lambert Land (Fig. 1) to the south of Blåsø and (2) input from the crystalline basement which crops out at the mouth of Nioghalvfjerdsfjorden on Hovgaard Ø (Fig. 1) (Smith et al., 2004a). Under both scenarios, the absence of the 79° N ice shelf would enable delivery of "exotic" lithologies via iceberg rafting either across or down the length of Nioghalvfjerdsfjorden. Irrespective of the source, the overall clay mineral composition of LF1 ($<$ smectite, $>$ illite, and variable chlorite and kaolinite) is considered to be a marine end-member.

Lithofacies 2 (LF2) is a black, stratified to laminated mud (Fig. 6). Both the grain size and magnetic susceptibility decrease relative to LF1, whereas Ti/Ca ratios increase markedly (Figs. 4, 5, 6). Br values remain low, and Mn/Fe values decrease and remain low. Smectite and kaolinite decrease with increases in illite and chlorite (Fig. 7). Foraminifera are absent in LF2, although low numbers

of chironomids (*Heterotrissocladius oliveri*-type) were observed.

A distinctive feature of LF2 is the change in the alkenone GC profiles, evident in the highly variable ketone indices (Fig. 8). The U_{37}^K generally decreases compared with LF1 but is variable. Values peak at 274 cm (0.2), decrease to -0.6 at 266 cm, and then increase to -0.1 at 258 cm (Fig. 8). $\%C_{37:4}$ is anticorrelated with U_{37}^K, with low values at 274 cm (11 %), peak values at 266 cm (67 %), and lower values at 258 cm (24 %). $\%C_{37:4}$ is generally higher relative to LF1. The variability in the K_{37}/K_{38} index decreases compared with LF1 and remains between 0.8 and 1.0. In addition to the distinctive ketone indices, the terrigenous OM progressively increases up to a peak at 268 cm (0.27 µg g^{-1}) before decreasing to previous concentrations. The aquatic OM increases to 0.05 µg g^{-1} and then slowly decreases towards the top of LF2 (0.03 µg g^{-1}). The TAR and C_{31}/C_{29} remain variable, both peaking around 270 cm. The CPI and pristane/phytane ratios remain low (values close to 1).

With respect to the palaeoenvironmental interpretation of LF2, the absence of foraminifera and the mix of alkenone producers (e.g. K_{37}/K_{38}; McClymont et al., 2005) coupled with an increase (decrease) in $\%C_{37:4}$ (U_{37}^K) indicate a shift to a cold, less-saline environment (Bendle and Rosell-Mele, 2004). We attribute these changes to the isolation of Blåsø as the 79° N ice shelf reformed and grounded at the western and eastern margins. The shift from an exclusively marine (LF1) to a fresher, less-saline water column occurs in steps, with the lowermost part of LF2 (280–274 cm) indicating that marine water still reached the core site and that the water column was well mixed. In contrast, above 274 cm, $\%C_{37:4}$ values imply a shift to a fresher water column and higher sea-ice concentrations.

Low Mn/Fe ratios, which also characterised the lower part of LF1 (Figs. 4, 5), indicate limited ventilation, which we attribute to increases in lake ice (as inferred from $> \%C_{37:4}$),

greater water column stratification, or a combination of both. Thicker lake ice would limit photosynthesis and exchange with the atmosphere – conditions that would be conducive to increased stratification and oxygen depletion. This is reflected in low Mn concentrations, indicative of Mn reduction under anoxic bottom-water conditions. Anoxic conditions would explain the black colour of LF2, and similar sediment characteristics have been recognised in other epishelf lake records, e.g. Disraeli Fiord (Antoniades et al., 2011), as marking a reduction in marine influence and a switch to freshwater dominance during ice shelf reformation. The suppression of biological activity expected from increasing lake ice is also supported by the presence of *Heterotrissocladius oliveri*-type chironomids, which are thought to live in the profundal zone and indicate a cold stenothermic (narrow temperature range) and possibly ultraoligotrophic environment (Winnell and White, 1986; Axford et al., 2019).

The transition from a largely marine to a fresher lacustrine setting is also accompanied by a change in producers, i.e. low K_{37}/K_{38} and increases in aquatic OM. Terrigenous inputs (terrigenous OM) increase between 274 and 250 cm, peaking during the freshest conditions at 268 cm (Fig. 8). This could be related to glacier advance providing a higher concentration of detritus or detritus from different sources, as indicated by the mix of OM signatures from vegetation (CPI, pristane/phytane, and C_{31}/C_{29}). The clay mineral data support variations in the sediment source. Both smectite and kaolinite decrease to minima at 268.5 cm and increase thereafter. This pattern is mirrored by increases (and decreases) in illite and chlorite. This variability likely reflects a transition from a marine clay mineral assemblage, whereby detritus is derived from multiple source areas, to one that is dominated by a local inputs (i.e. LF3). The input of terrigenous OM and the increase in aquatic OM imply enhanced lake fertilisation, and we envisage that the combination of increased nutrient flux and changes in water properties led to the change in producers at Blåsø.

LF3 is a red/brown, laminated, clay/silt with occasional > 2 mm clasts (Figs. 4, 5, 6). Some laminae are normally graded, with distinctive clay caps. Magnetic susceptibility gradually decreases up-core in LC12 (Fig. 5), whereas magnetic susceptibility first increases to ∼ 100 cm before decreasing in LC7 (Fig. 4). Minor increases in coarse silt occur in LC12 above 60 cm (Fig. 5). Illite remains the dominant clay mineral (> 50 %) but decreases relative to LF2 (Fig. 7). Smectite gradually decreases up-core from 11 % to 7 %, whereas kaolinite increases up to 180–120 cm (∼ 15 %) before decreasing again. Chlorite varies in the upper ∼ 60 cm but shows an overall increase in concentration up the core.

Foraminifera are generally absent, although rare tests occur in the upper 30 cm and in surface samples that contain calcareous and agglutinated species in very low abundances (*C. reniforme*, *E. excavatum*, and *Textularia earlandi*; Figs. 4, 5). Other microfauna include chironomids, Cyclorrhapha (flies), and copepods, although not in datable con-

centrations. Ti/Ca ratios drop in this unit but exhibit distinct variability between 0 and 0.05 (Figs. 4, 5).

The U_{37}^K decreases throughout LF3, ranging from between −0.4 and −0.7 in LF3a to between −0.6 and −0.7 in LF3b and LF3c. Conversely, $\%C_{37:4}$ increases from an average of 58 % in LF3a to 66 % in LF3b and LF3a. The uppermost sample, however, displays a higher U_{37}^K (−0.6) and lower $\%C_{37:4}$ (60 %) values. Similar changes are observed in the K_{37}/K_{38} index, which shows lower variability (values between 1.0 and 1.4) compared with LF1 and LF2, with one exception at 200 cm (where the index drops to 0.7), and a slow decreasing trend from an average of 1.2 in LF3a to 1.1 in LF3b and LF3c. Terrigenous and aquatic OM shows a gradual increasing trend throughout LF3a and greater variability in LF3b and LF3c. The CPI first increases in LF3a (from ∼ 1–1.3 up to 218 cm), reaches a broad maximum (1–1.2) between 218 and 128 cm, and then decreases through LF3b to low and stable values (0.7–0.8) in LF3c. The pristane/phytane ratio increases from below 1 to 3.7 at 218 cm and then shows an up-core decreasing trend, reaching values below 1 in LF3c. The C_{31}/C_{29} index is variable throughout LF3a (0.5–0.7) and progressively increases in LF3c and LF3c (0.6–1.0). The TAR displays low values (1.1–2.7) throughout LF3a and LF3b with a shift to increasing variability and higher values (2.5–5.5) in LF3c.

With respect to the palaeoenvironmental interpretation of LF3, the absence of foraminifera, except for rare occurrences in the upper ∼ 30 cm, and persistently high (low) $\%C_{37:4}$ (U_{37}^K) values imply that Blåsø remained largely isolated from marine water due to the persistence of an ice shelf. Recent analysis of Arctic surface sediments indicates that $\%C_{37:4}$ concentrations between 60 % and 70 % are typically associated with a ∼ 75 % sea-ice concentration (Wang et al., 2021). Thus, it seems likely that perennial lake ice existed in Blåsø which retarded, but did not completely stop, productivity in the surface water. The U_{37}^K values indicate warmer SWTs throughout much of LF3a, with a shift to cooler conditions in LF3b–LF3c (Fig. 8). A minor increase in temperature is observed in the upper ∼ 20 cm. The overall increase in aquatic and terrestrial OM in LF3a, indicative of higher woody vegetation (decreases in C_{31}/C_{29}), could imply a wetter climate (Bush and McInerney, 2013) that fertilised the surface waters in the summer melt season. An overall decrease in aquatic OM in LF3c, despite constant terrestrial OM input from higher grassy vegetation (increases in C_{31}/C_{29}), suggests less productivity in the lake, perhaps under drier conditions. The lower CPI and pristane / phytane ratios in LF3c likely reflect an increase in catchment erosion (Walinsky et al., 2009; Sánchez-Montes et al., 2020), although an increase in graminoids (Bush and McInerney, 2013) and more reductive conditions in the lake (Ten Haven et al., 1988) could also explain the low values. The higher TAR reflects increases in terrigenous OM and decreases in aquatic OM inputs across LF3. More generally, the laminated and graded nature of LF3 (potential varves; see Palmer et al., 2019) im-

plies seasonal variations in sediment input and/or different sediment sources (fluvial/fluviodeltaic vs. glacial).

As noted above, the clay mineral assemblage of LF3a–LF3b differs markedly from that deposited in a marine setting (LF1): LF3a–LF3b is characterised by > smectite, < illite, < chlorite, and > kaolinite. This reflects the lacustrine end-member, which was potentially isolated from exotic (marine) lithologies because of the ice shelf dam which would limit detritus delivered via IRD and/or sourced from a wider area. In this context, increases in smectite likely derive from the Neoproterozoic Rivieradal Group siliciclastic succession that contains conglomerates rich in quartzite and dolerite clasts (Higgins et al., 2004), with the latter likely to be smectite-rich. The higher kaolinite could derive from shales or limestones, which are also present in the Rivieradal Group and Odins Fjord Formation respectively.

One intriguing aspect of the upper ∼ 60 cm of LC12 (LC3c) is that it displays some of the characteristics of LF1 (e.g. increases in coarse silt, chlorite, illite, Br, and TAR as well as reduced CPI and aquatic OM), albeit with much lower numbers of foraminifera and %$C_{37:4}$ indicative of a "fresh" water column. Indeed, a minor increase in %$C_{37:4}$ from 58 % to 66 % and a decrease in U_{37}^{K} values at ∼ 100 cm imply decreasing SWTs and salinities. Taken at face value, this indicates that Blåsø became fresher, colder, and even more isolated from marine inputs above 100 cm. However, an alternative explanation is that the minor increase in foraminifera and the increases in clay minerals indicative of a marine end-member (Fig. 7) imply incursions of marine water to the central basin. While the %$C_{37:4}$ values preclude a fully mixed (marine) water column, the minor increase in foraminifera and other marine markers could reflect modern ice shelf thinning or thinning in the recent past, enabling a greater proportion of marine water into the central basin. This interpretation could explain the decrease in aquatic OM despite the continuous terrigenous inputs (increase in TAR and lower CPI). However, because we have not been able to date this part of the core (LF3a–LF3c), due to insufficient foraminifera/datable material, we cannot completely rule out that the marine signature reflects the reworking of uplifted glaciomarine sediments within the Blåsø catchment, possibly delivered to the lake by increased catchment erosion due to climate or glacier advance and/or aeolian transport.

4.2 Uplifted glaciomarine and deltaic sediments

Along the western and northern edge of Blåsø, uplifted glaciomarine (BUG) and deltaic sediments occur, some of which have previously been described by Bennike and Weidick (2001) (Figs. 2, 9, 10). Our field observations constrain the marine limit to ∼ 33 m a.s.l. (Figs. 9; 10a, b), although lake-ice push ridges were observed above this point up to ∼ 47 m a.s.l. To the west of Blåsø the marine limit is marked by an extensive coarse-gravel delta at ∼ 33 m a.s.l., and this

can be traced around the lake (Fig. 2). However, as the relative sea level fell through the Holocene, intermediate delta surfaces overprint the coastline at ∼ 25 and 15 m a.s.l. We identified two main lithofacies: BUG/LF1 and BUG/LF2.

BUG/LF1 comprises red/brown massive to weakly stratified clays and silts containing in situ macrofauna (articulated bivalves) dominated by *Hiatella arctica* (Figs. 9; 10c, d). In most exposures, this lithofacies occupies an elevational range of 0–22 m a.s.l. The predominance of silt and clay suggests that this is a deeper-water lithofacies which is distal to any ice-stream grounding line or local fluvial input. There are occasional dropstones indicative of ice-rafted input (Fig. 10e). Benthic foraminiferal assemblages, although not assessed quantitatively, are dominated by *E. clavatum* (Jennings et al., 2020) but also include several other glaciomarine and cold-water species (*C. reniforme*, *Islandiella islandica*, *Haynesina orbiculare*, *Astrononion gallowayi*, *Nonion* spp., *Triloculina tricarinata*, *S. feylingi*, *Spiroplectammina biformis*, and *Quinqueloculina* spp.). Therefore, BUG/LF1 is interpreted to reflect full glaciomarine conditions within the basin, with its fine-grained nature reflecting deeper-water conditions.

With respect to BUG/LF2, BUG/LF1 is overlain by planar bedded, well-sorted silty sand and fine gravel, as seen in Fig. 10f. These sediments become coarser in the upward direction and are characterised by planar cross-bedded and trough cross-bedded structures that we interpret as incised channels. These sediments form distinctive flat-topped surfaces at varying altitudes adjacent to the lake shore. These sediments contain both reworked and in situ molluscan fauna dominated by *Hiatella arctica* but with minor occurrences of *Astarte borealis* and *Mya truncata*. In several places around the lake, the upper sediment sequences are reworked into indistinct linear ridges. BUG/LF2 is interpreted as partially channelised, delta topsets which formed at the margins of the lake and overlying BUG/LF1. We envisage that the delta staircase formed at the periphery of the lake basin as relative sea level dropped from the marine limit at ∼ 33 to ∼ 25 m a.s.l. (SP2) and then to ∼ 15 m a.s.l. (SP1) (Fig. 9). The distinctive ridges are most likely lake-ice push ridges (Hendy et al., 2000). Similar landforms were seen forming along the contemporary lake edge during fieldwork in 2017.

4.3 Chronology

LF1 yielded foraminiferal (mixed benthic) ages of 4170–5670 ^{14}C yr BP (4056–5858 cal yr BP) for core LC7 and of 4345–5910 ^{14}C yr BP (4274–6127 cal yr BP) for core LC12 (Table 2). With the exception of one sample at 307 cm in core LC12, dated to 5910 ^{14}C yr BP, all ages occur in stratigraphic order within error. This age is omitted from our stratigraphy. Radiocarbon dating of the bulk organic fraction of LF1 and LF2 (LC12) yielded anomalously old ages (11 156–22 367 ^{14}C yr BP), likely reflecting the input of fossil carbon from the limestone-dominated catchment. Age–depth
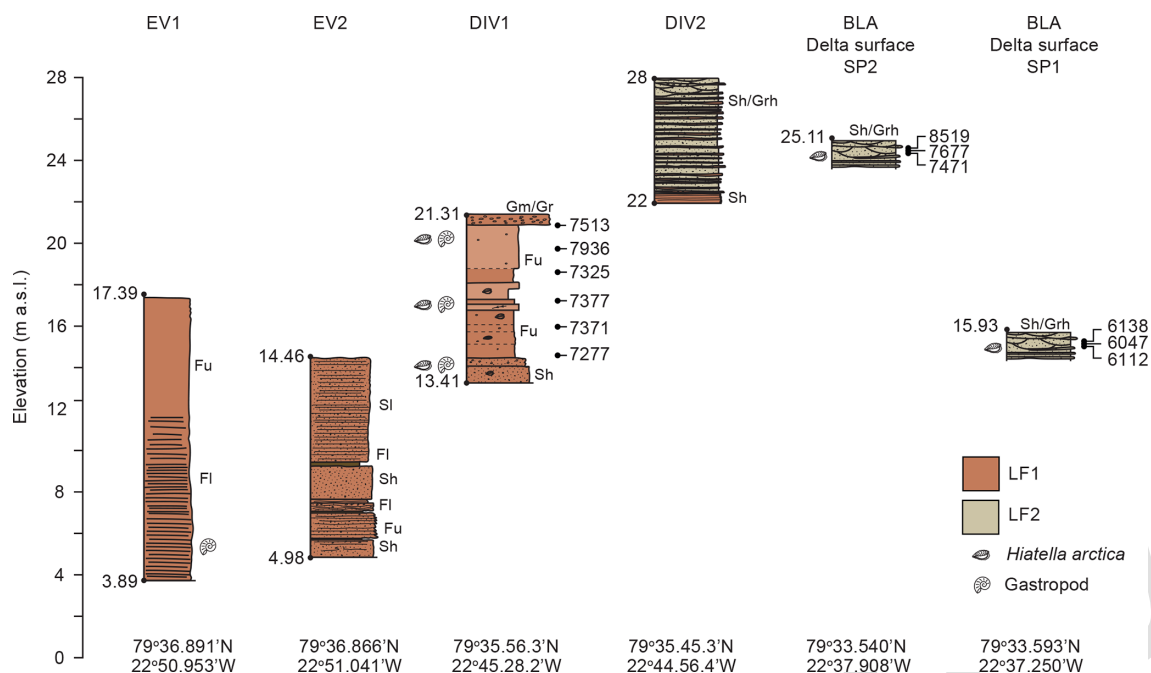
Figure 9. Altitudinal profile of the Blåsø uplifted glaciomarine and deltaic sediments (BUG). The abbreviations used in the figure are as follows: Gm – massive/crudely bedded gravel; Grh – horizontally bedded gravel; Gr – gravel, ripple cross-laminated; Sh – sheared/laminated sand; Fu – upward-fining mud; Fl – laminated mud/sand; and Sl – cross-bedded sand. Radiocarbon ages (cal yr BP) are shown to the right of section logs.

modelling of the ^{14}C age data (LF1) was undertaken with CLAM v2.40 using linear interpolation between neighbouring levels (Blaauw, 2010).

Shell samples (*Hiatella arctica* and gastropods) from the uplifted glaciomarine and deltaic sediments yielded ages of 5794–8205 ^{14}C yr BP (6022–8519 cal yr BP). BUG/LF1 is dated to 7227–7936 cal yr BP. It is older than LF1 recovered from the lake cores and, therefore, helps to constrain the initial phase of glaciomarine sedimentation in Blåsø. The sediments from BUG/LF2 record two separate phases of deltaic sedimentation at the periphery of the lake. The earliest deltaic phase is recorded at site SP2 at ∼ 25.11 m a.s.l. and is dated to 7629–8519 cal yr BP (Fig. 9). This is close to the marine limit and helps to constrain deglaciation, the early formation of Blåsø, and the onset of relative sea-level fall. A lower-elevation deltaic site (SP1 ∼ 15.93 m a.s.l.; Fig. 9) marks further sea-level fall constrained to 6022–6114 cal yr BP, and this also predates the deposition of LF1 in cores LC12 and LC7.

5 Discussion

The analysis of two sediment cores (LC7 and LC12) recovered from the central basin of Blåsø displays near-identical sedimentological, faunal, and geochemical/biomarker changes, thereby confirming a consistent history of deposition within the lake basin. Together with en-vironmental and chorological CE3 information from uplifted glaciomarine sediments, they provide a detailed record of the Early to Middle Holocene retreat of the 79° N ice shelf and its subsequent reformation. The discussion below mainly focuses on the results of LC12 because this core was analysed in most detail.

5.1 Ice shelf retreat phase (∼ 8.5 to 4.4 ka cal BP)

Raised glaciomarine deposits around Blåsø provide clear evidence of a complete deglaciation of the ∼ 70 km long Nioghalvfjerdsfjorden from a more advanced Late Glacial configuration (Fig. 11a; Winkelmann et al., 2010; Rasmussen et al., 2022). The onset of deglaciation – and the earliest evidence of the absence of the 79° N ice shelf – is constrained by the deposition of mollusc-bearing glaciomarine sediments (BUG/LF1). These sediments formed close to the marine limit (∼ 33 m a.s.l.) on the western side of Blåsø and have subsequently been uplifted due to isostatic rebound (Fig. 11b). Radiocarbon dating of in situ *Hiatella arctica* within BUG/LF1 indicates that marine conditions were established as early as ∼ 8.5 ka cal BP (Table 2). *Hiatella arctica* inhabits a relatively broad water depth range (0–800 m; Harbo, 1997), although the predominantly fine-grained nature of BUG/LF1 implies deposition in deeper water, distal to a grounding line. We envisage that BUG/LF1 formed as the relative sea level dropped from the marine limit at ∼ 33 m a.s.l. to ∼ 15 m a.s.l. (Fig. 11b). While the timing of
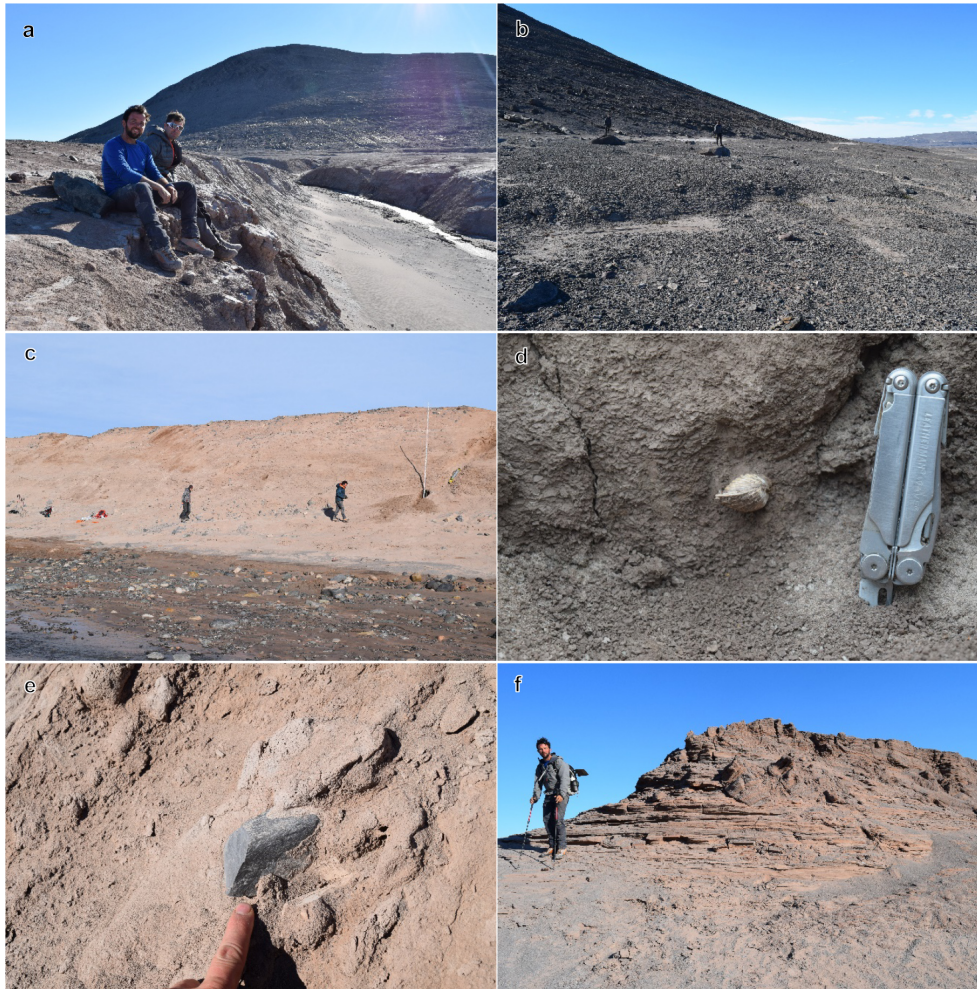
Figure 10. Photos of Blåsø uplifted glaciomarine (BUG) and deltaic sediments. Image **(a)** shows the uplifted glaciomarine sediments peripheral to Blåsø at site EV1. The marine limit at ∼ 33 m a.s.l. can be seen in the background. Below this, lithofacies BUG/LF1 is exposed due to local stream incision. Image **(b)** shows the marine limit at ∼ 33 m a.s.l. close to site EV1. Image **(c)** shows lithofacies BUG/LF1 sediments exposed at site DIV 1. These are predominantly massive to partially stratified red clay/silts with an assemblage of paired molluscs. They are capped by a thin layer of gravel. Image **(d)** presents a paired *Hiatella arctica* valve within lithofacies BUG/LF1 at site DIV1. Image **(e)** shows a striated dropstone in lithofacies BUG/LF1, indicating an ice-rafted component within this lithofacies. Image **(f)** shows lithofacies BUG/LF2 exposed at site DIV2 at 28 m a.s.l. This lithofacies varies in elevation but is characterised by planar and trough cross-bedded sand and gravels that often form distinctive flat surfaces peripheral to the Blåsø shoreline. Photographs were taken by David H. Roberts.

the sea-level drop is poorly constrained by our data, radiocarbon dating of gastropods within uppermost delta topsets records postglacial sea-level fall until ∼ 6.0 ka cal BP. The evidence of ice shelf absence between 8.5 and 4.0 ka cal BP is consistent with previously published ^{14}C dates from molluscs and whale bones which indicated that the ice shelf was smaller than present at ∼ 7.8–4.6 ka cal BP (Bennike and Weidick, 2001). The ages presented here extend the ice-free period by over a millennium. The chronology is also consistent with [10]Be ages which indicate that the deglaciation of Nioghalvfjerdsfjorden occurred between 9.2 and 7.9 ka (Larsen et al., 2018).

The lowermost sediments in LC12 and LC7 (LF1) are characterised by an exclusively open marine microfossil assemblage and alkenone profiles consistent with a fully mixed (saline) water column. This confirms that the ice shelf retreated and also provides additional insights into the environmental conditions close to the grounding line of 79° N Glacier. The ^{14}C data from LC7 and LC12 indicate that the Blåsø catchment was inundated by marine waters between 5.9 and 4.0 ka cal BP (Table 2). The foraminiferal fauna in both cores is characteristic of relatively "cold" Arctic water conditions, likely influenced by the input of glacial meltwater from nearby tidewater glacial margins as

Table 2. Compilation of radiocarbon (^{14}C) ages for cores LC7 and LC12 and uplifted glaciomarine sediments. "bf" refers to benthic and "AIOM" denotes acid-insoluble organic matter. All ^{14}C ages were corrected using a marine reservoir effect (MRE) of ~ 550 years (ΔR of 0 ± 0 years), following Hansen et al. (2022). Corrected ^{14}C ages were calibrated with the CALIB Radiocarbon Calibration program (version 8.1.0; http://calib.org/calib/, last access: 16 January 2023) using the Marine20 calibration curve (Heaton et al., 2020). Calibrated ages are given as a 2σ range (min, max, and mean).

Publication code	Sample ID	Depth (cm)	Material	Lithofacies	δ^{13}CVPDB‰ ± 0.1	^{14}C age (^{14}C yr BP)	±	ΔR	±	Calibrated age (cal yr BP) Min	Max	Mean
SUERC-90493	SC9	0	AIOM	LF3	−28.926	17 259	75	0	0	–	–	–
UCIAMS-211060	LC7	229	Mixed bf	LF1		4170	30	0	0	3881	4230	4056
BETA-499519	LC7	378.5	Mixed bf	LF1		5670	30	0	0	5690	6025	5858
SUERC-90494	LC7	202.5	AIOM	LF1	−29.902	15 211	63	0	0	–	–	–
UCIAMS-216429	LC12	279	Mixed bf	LF1		4345	30	0	0	4100	4447	4274
UCIAMS-216430	LC12	371	Mixed bf	LF1		4970	25	0	0	4858	5293	5076
SUERC-90482	LC12	11	AIOM	LF3c	−28.459	11 593	45	0	0	–	–	–
SUERC-90483	LC12	94.5	AIOM	LF3b	−28.174	18 388	85	0	0	–	–	–
SUERC-90484	LC12	183	AIOM	LF3a	−28.046	22 367	133	0	0	–	–	–
SUERC-90489	LC12	246	AIOM	LF3a	−28.554	15 864	65	0	0	–	–	–
SUERC-90490	LC12	263	AIOM	LF2	−27.864	11 156	45	0	0	–	–	–
SUERC-90491	LC12	297	AIOM	LF1	−27.005	12 074	47	0	0	–	–	–
SUERC-90492	LC12	326.5	AIOM	LF1	−28.047	14 011	55	0	0	–	–	–
UCIAMS-223836	LC12	307	Mixed bf	LF1		5910	30	0	0	5919	6302	6111
UCIAMS-223837	LC12	337	Mixed bf	LF1		4895	40	0	0	4789	5260	5025
UCIAMS-223840	LC12	347	Mixed bf	LF1		5035	35	0	0	4911	5399	5155
UCIAMS-225387	LC12	297	Mixed bf	LF1		4465	25	0	0	4209	4696	4453
UCIAMS-225388	LC12	327	Mixed bf	LF1		4705	25	0	0	4514	4961	4738
UCIAMS-225389	LC12	357	Mixed bf	LF1		5025	25	0	0	4892	5362	5127
SUERC-86006	Neg_Blaso_DIV_Sh01	–	*Hiatella arctica*	BUG/LF1	1.573	7168	38	0	0	7282	7634	7458
SUERC-86007	Neg_Blaso_DIV_Sh02	–	*Hiatella arctica*	BUG/LF1	0.695	7117	35	0	0	7241	7584	7413
SUERC-86008	Neg_Blaso_DIV_Sh03	–	*Hiatella arctica*	BUG/LF1	1.555	6958	36	0	0	7068	7452	7260
SUERC-86009	Neg_Blaso_DIV_Sh05	–	*Hiatella arctica*	BUG/LF1	0.621	7019	35	0	0	7147	7505	7326
SUERC-86013	Neg_Blaso_DIV_Sh013	–	*Hiatella arctica*	BUG/LF1	1.463	7012	35	0	0	7142	7502	7322
SUERC-86014	Neg_Blaso_DIV_Sh015	–	*Hiatella arctica*	BUG/LF1	1.395	6845	37	0	0	6937	7351	7144
UCIAMS-216453	Neg_Blaso_Delta_SP2A	–	Gastropod/bivalve	BUG/LF2		7420	50	0	0	7511	7904	7708
UCIAMS-216454	Neg_Blaso_Delta_SP2B	–	Gastropod/bivalve	BUG/LF2		7345	40	0	0	7442	7814	7628
SUERC-86015	Neg_Blaso_Delta_SP2C	–	Gastropod/bivalve	BUG/LF2	−0.538	8205	35	0	0	8320	8758	8539
SUERC-86016	Neg_Blaso_Delta_SP1A	–	Gastropod/bivalve	BUG/LF2	−0.272	5858	36	0	0	5885	6273	6079
SUERC-86017	Neg_Blaso_Delta_SP1B	–	Gastropod/bivalve	BUG/LF2	0.53	5794	37	0	0	5782	6214	5998
SUERC-86018	Neg_Blaso_Delta_SP1C	–	Gastropod/bivalve	BUG/LF2	−0.394	5900	38	0	0	5908	6298	6103

79° N Glacier readvanced and the ice shelf started to reform (Fig. 11c).

Multiple lines of evidence indicate that retreat of the 79° N ice shelf occurred at a time of atmospheric and ocean warming (Fig. 12). A compilation of ice core records and model simulations indicate that the most pronounced summer warming occurred from ~ 10 to 6 ka, i.e. during the HTM, and was roughly in phase but with lagging maximum summer insolation (Buizert et al., 2018). Maximum atmospheric warmth across Greenland is supported by chironomid-based temperature maxima at ~ 8–5 ka cal BP from a lake on nearby Store Koldewey (Klug et al., 2009). Similarly, marine records from the eastern Fram Strait as well as from directly in front of the 79° N ice shelf reveal a consistent picture of warm sea surface, subsurface, and bottom-water temperatures during the HTM. Foraminifera-based transfer functions indicate sea surface to subsurface temperatures of up to 6 °C until ~ 5 ka cal BP in the Fram Strait, with maximum seawater temperatures occurring from ~ 10 to 8 ka cal BP (Fig. 12; Werner et al., 2016). Assemblage data from the same core also indicate that Atlantic Water persisted in the Fram Strait between 10.6 and 8.5 ka cal BP, related

to maximum July insolation (Werner et al., 2016). Multi-proxy data from core PS100/270, 16 km from the calving front of the 79° N ice shelf (Fig. 11), indicate the strong inflow of warm recirculating Atlantic Water between ~ 10 and 7.5 ka cal BP (Syring et al., 2020), and this is consistent with foraminifera assemblage data from a core in the inner Norsk Trough that indicate a shift towards warmer conditions, an increase in nutrient supply, and higher productivity between 9.6 and 7.9 ka cal BP (Davies et al., 2022). The relative abundance of the Atlantic indicator *C. neoteretis* remains relatively high until approximately 6.5 ka cal BP in core PS100/270 but then decreases as the relatively cold-water indicator *C. reniforme* increases to over 40 % of the assemblage after ~ 6.0 ka cal BP (Syring et al., 2020).

Comparable environmental changes are also recorded in cores from the mid-shelf, where cold, sea-ice-covered surface waters and a strong subsurface influx of warm Atlantic water have been documented between ~ 9.4 and 8.2 ka cal BP (Pados-Dibattista et al., 2022). The authors also note a peak in IRD at ~ 8.4 ka cal BP that they attribute to the influx of terrestrially derived detritus associated with break-up of the 79° N ice shelf. These data are consistent with our obser-
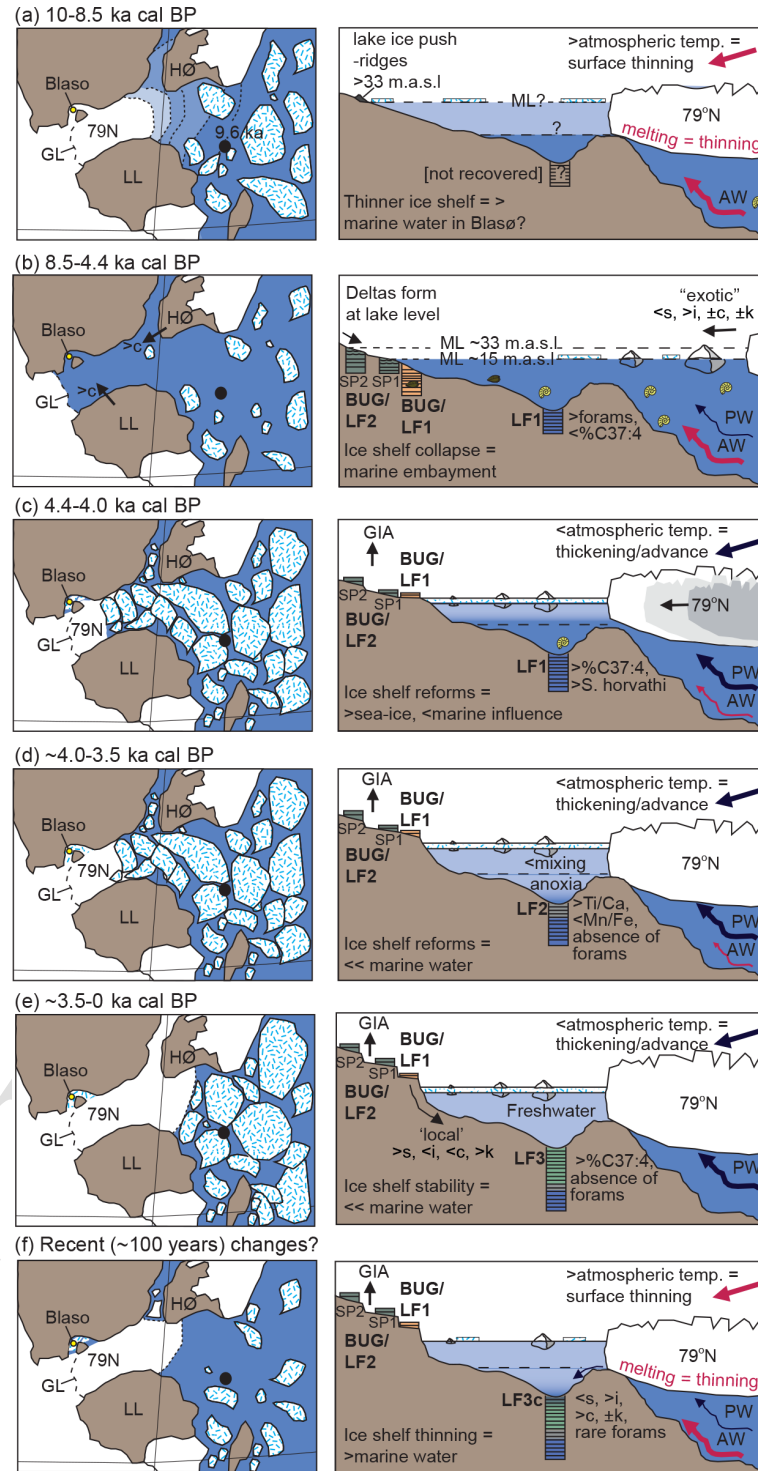
Figure 11. Reconstruction of the 79° N ice shelf from 10 ka cal BP to present, showing the location of Blåsø, Lambert Land (LL), and Hovgaard Ø (HØ). Constraints on sea-ice (blue-hatched polygons) formation and ocean circulation on the adjacent continental shelf (left column) are derived from core PS100/270 (closed black circle; Syring et al., 2020). Relative proportions of Atlantic Water (AW) and Polar Water (PW) are shown as thick/thin arrows. Conditions in Blåsø catchment (right column) prior to 8.5 ka cal BP (youngest shell age) are inferred. Relative proportions (> denotes high, < denotes low, and ± denotes variable) of the inferred pathways of smectite (s), illite (i), chlorite (c), and kaolinite (k) are indicated as well as the key attributes of lithofacies (LF) 1–3 in lake cores and Blåsø uplifted (BUG) lithofacies. Paler blue shading indicates more brackish/fresh water in Blåsø. ML stands for marine limit and GIA represents glacial isostatic adjustment. The yellow circle in Blåsø (left column) shows the relative positions of cores LC7 and LC12.
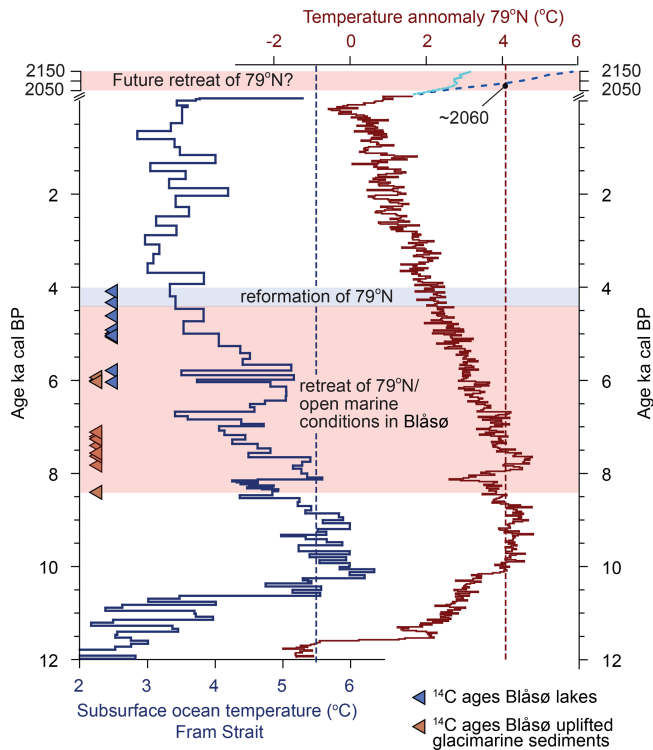
Figure 12. Marine conditions in Blåsø vs. atmospheric and ocean temperature. Ice shelf retreat (red shading) and reformation (blue shading) are constrained by ^{14}C ages (ka cal BP) of shell samples from uplifted glaciomarine sediments (brown triangles) and foraminiferal samples from LC12 and LC7 (light-blue triangles) in Blåsø. Subsurface ocean temperatures derived from planktic foraminiferal fauna assemblages (SST100) from core MSM5/5-723-2 are shown using the blue curve (Werner et al., 2016). Summer temperature (JJA) at 79° N based on data-model outputs is shown using the red curve (Buizert et al., 2018). Also shown are the Representative Concentration Pathway (RCP) 2.6 (dotted light-blue line) and 8.5 (dashed dark-blue line) scenarios (Hofer et al., 2020). Vertical dashed lines denote mean ocean (blue) and atmospheric (red) temperatures for the Early Holocene (∼ 10–8 ka). Under RCP8.5 (red shading), comparable Early Holocene atmospheric and ocean temperatures could occur by 2060.

vations of open marine conditions in Blåsø by 8.5 ka cal BP and, when viewed together with other proxy data, confirm that 79° N had retreated inboard of its present location after almost 2 millennia of elevated atmospheric and ocean tem-
5 peratures.

While the exact retreat configuration of 79° N Glacier and the 79° N ice shelf is unclear from our data, we suspect that grounding line retreat of the glacier was accompanied by ice shelf thinning, driven from above and below, leading to
10 eventual loss of the ice shelf in the Early Holocene and the formation of a tidewater calving margin, similar to the fate of Zachariæ Isstrøm after 2010 (Khan et al., 2014; Mouginot et al., 2015; An et al., 2021). Complete disintegration of the ice shelf is supported by the presence of driftwood

and whale and seal bones along Nioghalvfjerdsfjorden and 15 around the shore of Blåsø, dated to 7.7 and 4.5 ka cal BP (Bennike and Weidick, 2001). Thus, this trajectory of Early Holocene ice shelf loss seems similar to the present day, with enhanced basal and surface melting leading to ice shelf thinning and grounding line retreat. It is also possible that, af- 20 ter several centuries during which the mean annual temperatures exceeded current levels, extensive melt pools formed on the ice shelf surface (e.g. Turton et al., 2021) and eventually resulted in hydrofracture and catastrophic collapse of the ice shelf. Indeed, the glacial reconstruction of Syring et al. 25 (2020) indicates the retreat of an expanded 79° N ice shelf to a position similar to present after 9.6 ka cal BP, meaning that the ice shelf must have lost its entire area between ∼ 9.6 and 8.5 ka cal BP. It is likely that the collapse of the ice shelf during the Early to Middle Holocene was accompanied by a 30 retreat of 79° N Glacier, although the inland extent of this is unconstrained by our data and should be explored with an ice sheet model.

5.2 Ice shelf reformation phase and re-establishment of the epishelf lake at Blåsø (∼ 4.4 to 4.0 ka cal BP) 35

Our multi-proxy data set indicates a clear shift from an open (glaci)marine setting to one characterised by the increasing isolation of Blåsø from the marine water circulating in Nioghalvfjerdsfjorden. This started as a build-up of sea/lake ice after ∼ 4.4 ka cal BP, with increasing numbers of 40 *S. horvathi*, culminating in the complete isolation of Blåsø by 4.0 ka cal BP as the ice shelf thickened and re-grounded at the western and eastern ends of Blåsø (Fig. 11c). The combination of thick sea ice and the closure of Blåsø after ∼ 4.0 ka cal BP acted to limit photosynthesis and exchange 45 with the atmosphere and ocean; over the course of decades, this resulted in oxygen depletion and a period of anoxic conditions in the lake as well as lower aquatic productivity (Fig. 11d). Based on the interpolation of ^{14}C ages, the anoxic event lasted ∼ 500 years, i.e. until 3.5 ka cal BP, although this 50 is highly uncertain.

Grounding line advance is assumed to be accompanied by the reformation of the ice shelf, and this occurred at a time when proxy records indicate climate cooling (Fig. 12). In the Fram Strait, a weakened Atlantic Wa- 55 ter contribution occurs after ∼ 5.0 ka cal BP, when subsurface temperatures decrease rapidly (with minimum values observed between ∼ 4.0 and 3.0 ka cal BP) (Werner et al., 2016). On the continental shelf, Syring et al. (2020) document near-perennial sea-ice conditions with only short sum- 60 mers from ∼ 7.5 to ∼ 0.8 ka cal BP directly adjacent to the 79° N ice shelf, while Pados-Dibattista et al. (2022) suggested (near-)perennial sea-ice cover after ∼ 4.2 ka cal BP, associated with increased Polar Water at the surface of the East Greenland Current, and a reduction in the Re- 65 turn Atlantic Water at subsurface levels. Both ice core and chironomid-inferred records of atmospheric temperature in-

dicate that ocean cooling was accompanied by decreasing air temperatures (Buizert et al., 2018; Klug et al., 2009). Summer (June–July–August) temperatures at 79° N fall steadily from ∼ 7.9 ka cal BP, reaching ∼ 2.0 °C by 4.5 ka cal BP (Fig. 12) (Buizert et al., 2018). Similarly, the *Procladius* and *C. oliveri*-type chironomids decline in abundance in Duck Lake (Store Koldewey; Fig. 1a), which is likely related to deteriorating living conditions associated with the long-term decrease in summer air temperatures (Klug et al., 2009). In the absence of warm Atlantic Water circulating in the fiord and in the presence of declining air temperatures, it is likely that the grounding line advanced and the ice shelf reformed, probably as a composite ice shelf. The build-up of sea ice, potentially from as early as ∼ 7.5 ka cal BP (Syring et al., 2020), would have combined with increased snow accumulation (Rasmussen et al., 2013) to thicken and form multi-year sea/fast ice. This would have buttressed the ice shelf, allowing it to thicken and advance in tandem with the grounding line (Higgins, 1991; Robel, 2017). After ∼ 4.4 ka cal BP, the ice shelf had thickened and advanced sufficiently to begin impeding the circulation of marine waters in Blåsø, thus initiating the formation of the epishelf lake. The up-fiord advance of the ice shelf is poorly constrained by our data, but the absence of ages younger than ∼ 4.5 ka cal BP at "Midgård-sormen base camp" (Fig. 1) (Bennike and Weidick, 2001) suggests the ice shelf had advanced to at least this position. Given that the Midgårdsormen base camp is ∼ 15 km east of Blåsø's eastern mouth, the concurrent grounding of the ice shelf at both sites indicates that the ice shelf had started to reform and advance across the fiord well before ∼ 4.5 ka cal BP.

5.3 Epishelf lake phase (∼ 4.0 ka cal BP to present)

An epishelf lake was established by ∼ 4.0 ka cal BP, following continued (neoglacial) cooling (Fig. 11e). There is no indication of a return to marine-dominated conditions in Blåsø since then, suggesting that 79° N Glacier remained grounded at the western mouth of the lake and the rest of the fiord was continuously covered by an ice shelf from the Middle/Late Holocene to the present day. Throughout this period, Blåsø was likely covered by perennial lake ice, which appears to have been more dominant in the latter part of the record (upper 100 cm in LC12, LF3b, and LF3c; Fig. 5). Although uncertain, linear interpolation of the ^{14}C data indicates that LF3b and LF3c span the past ∼ 2 kyr. Despite the lack of a robust dating control, our multi-proxy data indicate variable sediment input into the lake, likely associated with catchment dynamics driven by climate variability. Wetter catchment conditions are inferred for LF3a/LF3b (increased aquatic and terrestrial OM, indicative of higher woody vegetation, and decreases in C_{31}/C_{29}; Meyers, 2003), while an overall decrease in aquatic OM and increases in C_{31}/C_{39} in LF3c (uppermost ∼ 60 cm) suggest less productivity in the lake, possibly during a drier climate. In the

nearby Trifna Sø catchment (Fig. 1a), 50 km north of Blåsø, soil erosion peaked at ∼ 3.4–3.0 ka cal BP, and the vegetation assemblage became more variable thereafter (Kusch et al., 2019). To the south, Duck Lake on Store Koldewey records a prolonged phase of lake-ice cover from 2.0 ka cal BP (Klug et al., 2009). In addition, high total inorganic carbon (TIC) values in Duck Lake between 1.3 and 0.8 ka cal BP, punctuated by a decrease at 1.0 ka cal BP, have been interpreted to represent phases of high productivity during periods of warmer summers. A similar pattern of high productivity separated by a drop in productivity has also been observed in other lake records from northeastern and East Greenland (Wagner and Melles, 2001; Wagner et al., 2000). On the adjacent mid-shelf, foraminiferal data imply cold and unstable oceanic conditions, with minimum surface water productivity and possible sea-ice cover from ∼ 3.2 until 0.3 ka cal BP (Pados-Dibattista et al., 2022). Pados-Dibattista et al. (2022) attributed this to a strengthened East Greenland Current resulting in a thick, cold, and fresh layer of Polar Water on the surface and strong recirculated Arctic Atlantic Water inflow at subsurface levels. Syring et al. (2020) pointed to a minimum solar insolation during the Middle to Late Holocene to explain the strengthened East Greenland Current and the influence of colder polar waters towards the inner shelf. It seems likely that some of the changes observed in Blåsø relate to regional climate variability, likely driven by changes in the atmospheric moisture content. While additional dating constraints are required in order to enable comparisons with other records, we suggest that generally wetter conditions persisted from ∼ 4 ka cal BP to ∼ 2 ka cal BP, with more variability and possibly a move to drier conditions recorded thereafter.

A final possibility – and one discussed above – is that the variability in proxies in the uppermost ∼ 60–50 cm of LC12 relates to the recent (past ∼ 100 years) thinning of 79° N allowing greater ingress of marine water (Fig. 11f). However, while the clay mineral assemblage shares similar attributes to the marine facies (LF1) and the presence of small numbers of calcareous microfossils could suggest renewed influence of marine water, the %$C_{37:4}$ ratios do not support increased salinity in the central basin. In this context, Bennike and Weidick (2001) have suggested that the 79° N ice shelf reached its maximum extent during the Little Ice Age (LIA) in response to neoglacial cooling. Thus, it is possible that some of the changes that we see in the upper ∼ 60 cm might relate to a reconfiguration of the ice shelf following LIA advance. In theory, this could introduce reworked uplifted glaciomarine sediments containing (Early/Middle Holocene age) foraminifera and a distinctive clay mineral signature. However, further work, with particular focus on dating the uppermost part of LC12, is required to decipher the significance of these changes.

5.4 Sensitivity of the 79° N ice shelf to post-LIA warming

Over the past decade, thinning and retreat of the floating portion of 79° N Glacier has raised concerns that its collapse is an inevitable consequence of continued climate warming. We show that past retreat of 79° N Glacier and collapse of its floating tongue occurred during the HTM, when atmospheric and ocean temperatures were similar to today, or within the projected scenarios of the Coupled Model Intercomparison Project, Phase 6, for the middle or end of this century (Fig. 12; Hofer et al., 2020). Specifically, the data-model reconstruction of Buizert et al. (2018) suggested that the HTM summer temperatures were ~ 3.3 °C above modern, although the mean annual temperatures were closer to ~ 2.0 °C above modern. While there is a lack of comparable ocean data, particularly proximal to 79° N, proxy-based reconstructions from the Fram Strait indicate that ocean temperatures during the HTM were ~ 2 °C warmer than historical data (1955–2012) (Werner et al., 2016). Currently, warm Atlantic Water from the Fram Strait is driven towards the glaciers in northeastern Greenland via Ekman pumping over the shelf break (Munchow et al., 2020), and it seems reasonable to assume similar processes operated in the past. In addition to being warmer, "peak" ocean and atmospheric temperatures during the HTM persisted for at least 1.7 and 1.4 ka respectively prior to the retreat of the 79° N ice shelf inboard of Blåsø (Fig. 12). The corollary of this is that the ice shelf was resilient under centuries to millennia of thermal forcing. However, it is worth noting that the HTM occurred while the ice sheet was retreating from a more advanced state, meaning that it was likely thicker and potentially more resilient to this past warm interval. Given the demise of neighbouring Zachariæ Isstrøm in 2015 (Mouginot et al., 2015) under intensified thermal forcing as well as the more recent collapse of Spalte Glacier in 2020, it seems reasonable to assume that the 79° N ice shelf will suffer the same fate. Taking the HTM ocean and atmospheric temperatures as a threshold for the loss of the 79° N ice shelf (acknowledging that this is likely an upper limit for this scenario), ~ 2.0 °C warming of the atmosphere may occur as early as 2060 (under high-emission scenarios, RCP8.5) (Fig. 12; Hofer et al., 2020), while ocean temperatures are also expected to reach 2.0 °C warmer than present by the end of the century (Yin et al., 2011). In this context, there is an urgent requirement for numerical modelling, utilising the timing of changes presented in this study as well as information on ocean and atmospheric forcing, to investigate the response of NEGIS to the retreat or loss of the ice shelf. Previous modelling work with fixed, present-day (atmospheric) seasonality could not produce a clear HTM minimum in the ice sheet extent (Lecavalier et al., 2014; Buizert et al., 2018). The inability of the latter models to drive significant GrIS retreat likely relates to the lack of ocean forcing (Buizert et al., 2018). Indeed, most ice sheet numerical models used to project sea-level rise from the GrIS do not include realistic ocean thermal forcing (Goelzer et al., 2020); thus, this needs to be included in future model simulations.

6 Conclusions

High-resolution, multi-proxy sediment records from an epishelf lake in northeast Greenland and dating of marine molluscs from uplifted glaciomarine sediments show that the 79° N ice shelf was ~ 70 km inboard of the present ice shelf margin during the Early to Middle Holocene (between ~ 8.5 and 4.4 ka cal BP). Ice shelf collapse was also likely to have been accompanied by retreat of 79° N Glacier, although the inland extent of this is unconstrained by our data.

The timing of ice shelf retreat through Nioghalvfjerdsfjorden followed a period of thermal forcing when atmospheric and ocean temperatures were > 2 °C warmer than present and were sustained for at least a millennium prior to ice shelf collapse/retreat. While this implies some resilience to thermal forcing, the ice sheet/shelf was retreating from an advanced position following the Last Glacial Maximum, meaning that it was likely thicker and potentially more resistant to climate change during the Early Holocene.

The ice shelf reformed from ~ 4.4 to 4.0 ka cal BP during a phase of climatic cooling, although the precise spatial pattern of reformation is not known. We speculate that the ice shelf reformed via the thickening of sea ice, which helped buttress and thicken an advancing ice tongue.

Our reconstruction suggests that the 79° N ice shelf is vulnerable to collapse when atmospheric and ocean temperatures are > 2 °C warmer than present, which could be achieved by the middle of this century under some climate model scenarios.

Finally, the uppermost ~ 60 cm of the epishelf lake core record displays characteristics similar to those observed during the Early Holocene collapse. This could suggest that recent thinning of the 79° N ice shelf is now detected in Blåsø, although further work – particularly focusing on generating new age constraints – is required to test this hypothesis.

Data availability. Chronological and sedimentological data for cores LC7 and LC12 from Blåsø (Smith et al., 2022) are available from the UK NERC Polar Data Centre (https://doi.org/10.5285/e44bbc45-9924-401b-a7b8-7939fbb61db2, Smith et al., 2022).

Author contributions. JAS, MJB, DRH, SJ, JML, BRR, and CO conceived the study. JAS wrote the initial draft of the manuscript. JAS, MJB, SJ, and TL recovered the lake sediment cores, and DHR, JAS, MJB, TL, and CD sampled the uplifted glaciomarine sediments. LC split, described, sampled, and performed the non-destructive analyses (physical properties, XRF scanning) of the lake core, with help from DHR and JAS. JML undertook the

foraminiferal work, MLS performed the biomarker analyses with ELM, WE analysed the clay minerals, and PG performed the ^{14}C dating at SUERC. All authors discussed the results and implications and collaborated on writing the manuscript.

Competing interests. The contact author has declared that none of the authors has any competing interests.

Acknowledgements. This work was funded by a NERC standard grant (grant no. NE/N011228/1), and some radiocarbon analysis was funded by NEIF (grant NE/S011587/1; allocation number 2169.1118). We thank the Alfred Wegener Institute, particularly Angelika Humbert and Hicham Rafiq, for significant logistic support through the iGRIFF project. Additional support was provided by Station Nord (Jorgen Skafte), Nordlandair, Air Greenland, and the Joint Arctic Command. Naalakkersuisut (government of Greenland) provided scientific survey (VU-00121) and export (046/2017) licences for this work. Finally, we would like to thank our (Nanu Travel) field ranger Isak (and dog Ooni) for keeping us safe in the field and taking great pleasure in beating James A. Smith at cards.

Financial support. This research has been supported by the Natural Environment Research Council (grant no. NE/N011228/1).

Review statement. This paper was edited by Florence Colleoni and reviewed by Anne Jennings and one anonymous referee.

References

An, L., Rignot, E., Wood, M., Willis, J. K., Mouginot, J., and Khan, S. A.: Ocean melting of the Zachariae Isstrom and Nioghalvfjerdsfjorden glaciers, northeast Greenland, P. Natl. Acad. Sci. USA, 118, https://doi.org/10.1073/pnas.2015483118, 2021.

Antoniades, D., Francus, P., Pienitz, R., St-Onge, G., and Vincent, W. F.: Holocene dynamics of the Arctic's largest ice shelf, P. Natl. Acad. Sci. USA, 108, 18899–18904, https://doi.org/10.1073/pnas.1106378108, 2011.

Arz, H., Patzold, J., and Wefer, G.: Climatic changes during the last deglaciation recorded in sediment cores from the northeastern Brazilian Continental Margin, Geo-Mar. Lett., 19, 209–218, 1999.

Aschwanden, A., Fahnestock, M. A., Truffer, M., Brinkerhoff, D. J., Hock, R., Khroulev, C., Mottram, R., and Khan, S. A.: Contribution of the Greenland Ice Sheet to sea level over the next millennium, Science Advances, 5, eaav9396, https://doi.org/10.1126/sciadv.aav9396, 2019.

Axford, Y., Lasher, G. E., Kelly, M. A., Osterberg, E. C., Landis, J., Schellinger, G. C., Pfeiffer, A., Thompson, E., and Francis, D. R.: Holocene temperature history of northwest Greenland – With new ice cap constraints and chironomid assemblages from Deltaso, Quaternary Sci. Rev., 215, 160–172, https://doi.org/10.1016/j.quascirev.2019.05.011, 2019.

Bahr, A., Lamy, F., Arz, H., Kuhlmann, H., and Wefer, G.: Late glacial to Holocene climate and sedimentation history in the NW Black Sea, Mar. Geol., 214, 309–322, https://doi.org/10.1016/j.margeo.2004.11.013, 2005.

Bendle, J. and Rosell-Mele, A.: Distributions of U^K_{37} and $U^K_{37'}$ in the surface waters and sediments of the Nordic Seas: Implications for paleoceanography, Geochem. Geophy. Geosy., 5, Q11013, https://doi.org/10.1029/2004gc000741, 2004.

Bennike, O. and Weidick, A.: Late Quaternary history around Nioghalvfjerdsfjorden and Jokelbugten, North-East Greenland, Boreas, 30, 205–227, https://doi.org/10.1111/j.1502-3885.2001.tb01223.x, 2001.

Bentley, M. J., Hodgson, D. A., Sugden, D. E., Roberts, S. J., Smith, J. A., Leng, M. J., and Bryant, C.: Early Holocene retreat of the George VI Ice Shelf, Antarctic Peninsula, Geology, 33, 173–176, https://doi.org/10.1130/g21203.1, 2005.

Bentley, M. J., Smith, J. A., Jamieson, S. S. R., Lindeman, M., Rea, B. R., Humbert, A., Lane, T. P., Darvill, C. M., Lloyd, J. M., Straneo, F., Helm, V., and Roberts, D. H.: Direct measurement of warm Atlantic Intermediate Water close to the grounding line of Nioghalvfjerdsfjorden (79N) Glacier, North-east Greenland, The Cryosphere Discuss. [preprint], https://doi.org/10.5194/tc-2022-206, in review, 2022.

Blaauw, M.: Methods and code for 'classical' age-modelling of radiocarbon sequences, Quat. Geochronol., 5, 512–518, https://doi.org/10.1016/j.quageo.2010.01.002, 2010.

Blau, M. T., Turton, J. V., Sauter, T., and Molg, T.: Surface mass balance and energy balance of the 79N Glacier (Nioghalvfjerdsfjorden, NE Greenland) modeled by linking COSIPY and Polar WRF, J. Glaciol., 67, 1093–1107, https://doi.org/10.1017/jog.2021.56, 2021.

Bray, E. E. and Evans, E. D.: Distribution of *n*-paraffins as a clue to recognition of source beds, Geochim. Cosmochim. Ac., 22, 2–15, https://doi.org/10.1016/0016-7037(61)90069-2, 1961.

Buizert, C., Keisling, B. A., Box, J. E., He, F., Carlson, A. E., Sinclair, G., and DeConto, R. M.: Greenland-Wide Seasonal Temperatures During the Last Deglaciation, Geophys. Res. Lett., 45, 1905–1914, https://doi.org/10.1002/2017GL075601, 2018.

Bush, R. T. and McInerney, F. A.: Leaf wax n-alkane distributions in and across modern plants: Implications for paleoecology and chemotaxonomy, Geochim. Cosmochim. Ac., 117, 161–179, https://doi.org/10.1016/j.gca.2013.04.016, 2013.

Cage, A. G., Pieńkowski, A. J., Jennings, A., Knudsen, K. L., and Seidenkrantz, M.-S.: Comparative analysis of six common foraminiferal species of the genera *Cassidulina*, *Paracassidulina*, and *Islandiella* from the Arctic–North Atlantic domain, J. Micropalaeontol., 40, 37–60, https://doi.org/10.5194/jm-40-37-2021, 2021.

Choi, Y., Morlighem, M., Rignot, E., Mouginot, J., and Wood, M.: Modeling the Response of Nioghalvfjerdsfjorden and Zachariae Isstrom Glaciers, Greenland, to Ocean Forcing Over the Next Century, Geophys. Res. Lett., 44, 11071–11079, https://doi.org/10.1002/2017gl075174, 2017.

Consolaro, C., Rasmussen, T. L., and Panieri, G.: Palaeoceanographic and environmental changes in the eastern Fram

Strait during the last 14,000 years based on benthic and planktonic foraminifera, Mar. Micropaleontol., 139, 84–101, https://doi.org/10.1016/j.marmicro.2017.11.001, 2018.

Cranwell, P. A.: Branched-chain and cyclopropanoid acids in a recent sediment, Chem. Geol., 11, 307–313, https://doi.org/10.1016/0009-2541(73)90101-0, 1973.

D'Andrea, W. J., Huang, Y. S., Fritz, S. C., and Anderson, N. J.: Abrupt Holocene climate change as an important factor for human migration in West Greenland, P. Natl. Acad. Sci. USA, 108, 9765–9769, https://doi.org/10.1073/pnas.1101708108, 2011.

Davies, J., Mathiasen, A. M., Kristiansen, K., Hansen, K. E., Wacker, L., Alstrup, A. K. O., Munk, O. L., Pearce, C., and Seidenkrantz, M.-S.: Linkages between ocean circulation and the Northeast Greenland Ice Stream in the Early Holocene, Quaternary Sci. Rev., 286, 107530, https://doi.org/10.1016/j.quascirev.2022.107530, 2022.

Ehrmann, W., Hillenbrand, C.-D., Smith, J. A., Graham, A. G. C., Kuhn, G., and Larter, R. D.: Provenance changes between recent and glacial-time sediments in the Amundsen Sea embayment, West Antarctica: clay mineral assemblage evidence, Antarct. Sci., 23, 471–486, https://doi.org/10.1017/s0954102011000320, 2011.

Evans, D. and Benn, D. I.: A Practical Guide to the Study of Glacial Sediments, Edward Arnold, London, ISBN 0-340-75959-3, 2004.

Fettweis, X., Box, J. E., Agosta, C., Amory, C., Kittel, C., Lang, C., van As, D., Machguth, H., and Gallée, H.: Reconstructions of the 1900–2015 Greenland ice sheet surface mass balance using the regional climate MAR model, The Cryosphere, 11, 1015–1033, https://doi.org/10.5194/tc-11-1015-2017, 2017.

Funder, S.: ^{14}C-dating of samples collected during the 1979 expedition to North Greenland, The Geological Survey of Greenland Report 110, 9–13, 1982.

Goelzer, H., Nowicki, S., Payne, A., Larour, E., Seroussi, H., Lipscomb, W. H., Gregory, J., Abe-Ouchi, A., Shepherd, A., Simon, E., Agosta, C., Alexander, P., Aschwanden, A., Barthel, A., Calov, R., Chambers, C., Choi, Y., Cuzzone, J., Dumas, C., Edwards, T., Felikson, D., Fettweis, X., Golledge, N. R., Greve, R., Humbert, A., Huybrechts, P., Le clec'h, S., Lee, V., Leguy, G., Little, C., Lowry, D. P., Morlighem, M., Nias, I., Quiquet, A., Rückamp, M., Schlegel, N.-J., Slater, D. A., Smith, R. S., Straneo, F., Tarasov, L., van de Wal, R., and van den Broeke, M.: The future sea-level contribution of the Greenland ice sheet: a multimodel ensemble study of ISMIP6, The Cryosphere, 14, 3071–3096, https://doi.org/10.5194/tc-14-3071-2020, 2020.

Guillemot, T., Bichet, V., Gauthier, E., Zocatelli, R., Massa, C., and Richard, H.: Environmental responses of past and recent agropastoral activities on south Greenlandic ecosystems through molecular biomarkers, Holocene, 27, 783–795, https://doi.org/10.1177/0959683616675811, 2017.

Hald, M. and Korsun, S.: Distribution of modern benthic foraminifera from fjords of Svalbard, European Arctic, J. Foramin. Res., 27, 101–122, https://doi.org/10.2113/gsjfr.27.2.101, 1997.

Hanna, E., Cappelen, J., Fettweis, X., Mernild, S. H., Mote, T. L., Mottram, R., Steffen, K., Ballinger, T. J., and Hall, R.: Greenland surface air temperature changes from 1981 to 2019 and implications for ice-sheet melt and mass-balance change, Int. J. Climatol., 41, E1336–E1352, https://doi.org/10.1002/joc.6771, 2021.

Hansen, K. E., Lorenzen, J., Davies, J., Wacker, L., Pearce, C., and Seidenkrantz, M.-S.: Deglacial to Mid Holocene environmental conditions on the northeastern Greenland shelf, western Fram Strait, Quat. Sci. Rev., 293, 107704, https://doi.org/10.1016/j.quascirev.2022.107704, 2022.

Harbo, R. M.: Shells and shellfish of the Pacific Northwest, a field guide, Harbour Publishing, Canada, 1–270, 1997.[TS1]

Heaton, T. J., Köhler, P., Butzin, M., Bard, E., Reimer, R. W., Austin, W. E. N., Bronk Ramsey, C., Grootes, P. M., Hughen, K. A., Kromer, B., Reimer, P. J., Adkins, J., Burke, A., Cook, M. S., Olsen, J., and Skinner, L. C.: Marine20—The Marine Radiocarbon Age Calibration Curve (0–55,000 cal BP), Radiocarbon, 62, 779–820, https://doi.org/10.1017/RDC.2020.68, 2020.

Heaton, T. J., Bard, E., Bronk Ramsey, C., Butzin, M., Hatté, C., Hughen, K. A., Köhler, P., and Reimer, P. J.: A RESPONSE TO COMMUNITY QUESTIONS ON THE MARINE20 RADIOCARBON AGE CALIBRATION CURVE: MARINE RESERVOIR AGES AND THE CALIBRATION OF ^{14}C SAMPLES FROM THE OCEANS, Radiocarbon, 1–27, https://doi.org/10.1017/RDC.2022.66, 2022.

Hendy, C. H., Sadler, A. J., Denton, G. H., and Hall, B. L.: Proglacial lake-ice conveyors: A new mechanism for deposition of drift in polar environments, Geogr. Ann. A, 82A, 249–270, 2000.

Higgins, A. and Kalsbeek, F.: East Greenland Caledonides: stratigraphy, structure and geochronology, Geol. Surv. Den. Greenl., 6, 1–96, https://doi.org/10.34194/geusb.v6.4814, 2004.

Higgins, A. K.: North Greenland glacier velocities and calf ice production, Polarforschung, 60, 1–23, 1991.

Higgins, A. K., Soper, N. J., Smith, M. P., and Rasmussen, J. A.: The Caledonian thin-skinned thrust belt of Kronprins Christian Land, eastern North Greenland, Geol. Surv. Den. Greenl., 6, 41–56, https://doi.org/10.34194/geusb.v6.4817, 2004.

Hochreuther, P., Neckel, N., Reimann, N., Humbert, A., and Braun, M.: Fully Automated Detection of Supraglacial Lake Area for Northeast Greenland Using Sentinel-2 Time-Series, Remote Sens.-Basel, 13, 205, https://doi.org/10.3390/rs13020205, 2021.

Hofer, S., Lang, C., Amory, C., Kittel, C., Delhasse, A., Tedstone, A., and Fettweis, X.: Greater Greenland Ice Sheet contribution to global sea level rise in CMIP6, Nat. Commun., 11, 6289, https://doi.org/10.1038/s41467-020-20011-8, 2020.

Jennings, A., Andrews, J., and Wilson, L.: Holocene environmental evolution of the SE Greenland Shelf North and South of the Denmark Strait: Irminger and East Greenland current interactions, Quaternary Sci. Rev., 30, 980–998, https://doi.org/10.1016/j.quascirev.2011.01.016, 2011.

Jennings, A., Andrews, J., Reilly, B., Walczak, M., Jakobsson, M., Mix, A., Stoner, J., Nicholls, K. W., and Cheseby, M.: Modern foraminiferal assemblages in northern Nares Strait, Petermann Fjord, and beneath Petermann ice tongue, NW Greenland, Arct. Antarct. Alp. Res., 52, 491–511, https://doi.org/10.1080/15230430.2020.1806986, 2020.

Jennings, A. E., Weiner, N. J., Helgadottir, G., and Andrews, J. T.: Modern foraminiferal faunas of the southwestern to northern Iceland shelf: Oceanographic and environmental controls, J. Foramin. Res., 34, 180–207, https://doi.org/10.2113/34.3.180, 2004.

Joughin, I., Smith, B. E., Howat, I. M., Scambos, T., and Moon, T.: Greenland flow variability from ice-

sheet-wide velocity mapping, J. Glaciol., 56, 415–430, https://doi.org/10.3189/002214310792447734, 2010.

Khan, S. A., Kjaer, K. H., Bevis, M., Bamber, J. L., Wahr, J., Kjeldsen, K. K., Bjork, A. A., Korsgaard, N. J., Stearns, L. A., van den Broeke, M. R., Liu, L., Larsen, N. K., and Muresan, I. S.: Sustained mass loss of the northeast Greenland ice sheet triggered by regional warming, Nat. Clim. Change, 4, 292–299, https://doi.org/10.1038/nclimate2161, 2014.

Klug, M., Schmidt, S., Bennike, O., Heiri, O., Melles, M., and Wagner, B.: Lake sediments from Store Koldewey, Northeast Greenland, as archive of Late Pleistocene and Holocene climatic and environmental changes, Boreas, 38, 59–71, https://doi.org/10.1111/j.1502-3885.2008.00038.x, 2009.

Kornilova, O. and Rosell-Mele, A.: Application of microwave-assisted extraction to the analysis of biomarker climate proxies in marine sediments, Org. Geochem., 34, 1517–1523, https://doi.org/10.1016/s0146-6380(03)00155-4, 2003.

Kusch, S., Bennike, O., Wagner, B., Lenz, M., Steffen, I., and Rethemeyer, J.: Holocene environmental history in high-Arctic North Greenland revealed by a combined biomarker and macrofossil approach, Boreas, 48, 273–286, https://doi.org/10.1111/bor.12377, 2019.

Larsen, N. K., Levy, L. B., Carlson, A. E., Buizert, C., Olsen, J., Strunk, A., Bjork, A. A., and Skov, D. S.: Instability of the North-east Greenland Ice Stream over the last 45,000 years, Nat. Commun., 9, https://doi.org/10.1038/s41467-018-04312-7, 2018.

Lecavalier, B. S., Milne, G. A., Simpson, M. J. R., Wake, L., Huybrechts, P., Tarasov, L., Kjeldsen, K. K., Funder, S., Long, A. J., Woodroffe, S., Dyke, A. S., and Larsen, N. K.: A model of Greenland ice sheet deglaciation constrained by observations of relative sea level and ice extent, Quaternary Sci. Rev., 102, 54–84, https://doi.org/10.1016/j.quascirev.2014.07.018, 2014.

Leeson, A. A., Shepherd, A., Briggs, K., Howat, I., Fettweis, X., Morlighem, M., and Rignot, E.: Supraglacial lakes on the Greenland ice sheet advance inland under warming climate, Nat. Clim. Change, 5, 51–55, https://doi.org/10.1038/nclimate2463, 2015.

Mayer, C., Schaffer, J., Hattermann, T., Floricioiu, D., Krieger, L., Dodd, P. A., Kanzow, T., Licciulli, C., and Schannwell, C.: Large ice loss variability at Nioghalvfjerdsfjorden Glacier, Northeast-Greenland, Nat. Commun., 9, 2768, https://doi.org/10.1038/s41467-018-05180-x, 2018.

McClymont, E. L., Rosell-Mele, A., Giraudeau, J., Pierre, C., and Lloyd, J. M.: Alkenone and coccolith records of the mid-Pleistocene in the south-east Atlantic: Implications for the $U_{37}^{K'}$ index and South African climate, Quaternary Sci. Rev., 24, 1559–1572, https://doi.org/10.1016/j.quascirev.2004.06.024, 2005.

Meyers, P. A.: Applications of organic geochemistry to paleolimnological reconstructions: a summary of examples from the Laurentian Great Lakes, Org. Geochem., 34, 261–289, https://doi.org/10.1016/s0146-6380(02)00168-7, 2003.

Morlighem, M., Williams, C. N., Rignot, E., An, L., Arndt, J. E., Bamber, J. L., Catania, G., Chauche, N., Dowdeswell, J. A., Dorschel, B., Fenty, I., Hogan, K., Howat, I., Hubbard, A., Jakobsson, M., Jordan, T. M., Kjeldsen, K. K., Millan, R., Mayer, L., Mouginot, J., Noel, B. P. Y., O'Cofaigh, C., Palmer, S., Rysgaard, S., Seroussi, H., Siegert, M. J., Slabon, P., Straneo, F., van den Broeke, M. R., Weinrebe, W., Wood, M., and Zinglersen, K. B.: BedMachine v3: Complete Bed Topography and Ocean Bathymetry Mapping of Greenland From Multibeam Echo Sounding Combined With Mass Conservation, Geophys. Res. Lett., 44, 11051–11061, https://doi.org/10.1002/2017gl074954, 2017.

Mottram, R., B. Simonsen, S., Høyer Svendsen, S., Barletta, V. R., Sandberg Sørensen, L., Nagler, T., Wuite, J., Groh, A., Horwath, M., Rosier, J., Solgaard, A., Hvidberg, C. S., and Forsberg, R.: An Integrated View of Greenland Ice Sheet Mass Changes Based on Models and Satellite Observations, Remote Sens.-Basel, 11, 1407, https://doi.org/10.3390/rs11121407, 2019.

Mouginot, J., Rignot, E., Scheuchl, B., Fenty, I., Khazendar, A., Morlighem, M., Buzzi, A., and Paden, J.: Fast retreat of Zachariæ Isstrøm, northeast Greenland, Science, 350, 1357–1361, https://doi.org/10.1126/science.aac7111, 2015.

Munchow, A., Schaffer, J., and Kanzow, T.: Ocean Circulation Connecting Fram Strait to Glaciers off Northeast Greenland: Mean Flows, Topographic Rossby Waves, and Their Forcing, J. Phys. Oceanogr., 50, 509–530, https://doi.org/10.1175/jpo-d-19-0085.1, 2020.

Nace, T. E., Baker, P. A., Dwyer, G. S., Silva, C. G., Rigsby, C. A., Burns, S. J., Giosan, L., Otto-Bliesner, B., Liu, Z. Y., and Zhu, J.: The role of North Brazil Current transport in the paleoclimate of the Brazilian Nordeste margin and paleoceanography of the western tropical Atlantic during the late Quaternary, Palaeogeogr. Palaeocl., 415, 3–13, https://doi.org/10.1016/j.palaeo.2014.05.030, 2014.

Naeher, S., Gilli, A., North, R. P., Hamann, Y., and Schubert, C. J.: Tracing bottom water oxygenation with sedimentary Mn/Fe ratios in Lake Zurich, Switzerland, Chem. Geol., 352, 125–133, https://doi.org/10.1016/j.chemgeo.2013.06.006, 2013.

Nick, F. M., Van Der Veen, C. J., Vieli, A., and Benn, D. I.: A physically based calving model applied to marine outlet glaciers and implications for the glacier dynamics, J. Glaciol., 56, 781–794, https://doi.org/10.3189/002214310794457344, 2010.

O'Regan, M., Cronin, T. M., Reilly, B., Alstrup, A. K. O., Gemery, L., Golub, A., Mayer, L. A., Morlighem, M., Moros, M., Munk, O. L., Nilsson, J., Pearce, C., Detlef, H., Stranne, C., Vermassen, F., West, G., and Jakobsson, M.: The Holocene dynamics of Ryder Glacier and ice tongue in north Greenland, The Cryosphere, 15, 4073–4097, https://doi.org/10.5194/tc-15-4073-2021, 2021.

Oppenheimer, M., Glavovic, B., Hinkel, J., van deWal, R., Magnan, A. K., Abd-Elgawad, A., Cai, R., Cifuentes-Jara, M., Deconto, R. M., Ghosh, T., Hay, J., Isla, F., Marzeion, B., Meyssignac, B., and Sebesvari, Z.: Sea Level Rise and Implications for Low-Lying Islands, Coasts and Communities, in: IPCC Special Report on the Ocean and Cryosphere in a Changing Climate, edited by: Po¨rtner, H.-O., Roberts, D. C., Masson-Delmotte, V., Zhai, P., Tignor, M., Poloczanska, E., Mintenbeck, K., Alegri´a, A., M. Nicolai, M., Okem, A., Petzold, J., Rama, B., and Weyer, N. M., Cambridge University Press, Cambridge, 321–445, https://doi.org/10.1017/9781009157964.006, 2019.

Pados-Dibattista, T., Pearce, C., Detlef, H., Bendtsen, J., and Seidenkrantz, M.-S.: Holocene palaeoceanography of the Northeast Greenland shelf, Clim. Past, 18, 103–127, https://doi.org/10.5194/cp-18-103-2022, 2022.

Palmer, A. P., Bendle, J. M., MacLeod, A., Rose, J., and Thorndycraft, V. R.: The micromorphology of glaciolacustrine varve sediments and their use for reconstructing palaeoglaciological and palaeoenvironmental change, Quaternary Sci. Rev., 226, 105964, https://doi.org/10.1016/j.quascirev.2019.105964, 2019.

Perner, K., Moros, M., Lloyd, J. M., Kuijpers, A., Telford, R. J., and Harff, J.: Centennial scale benthic foraminiferal record of late Holocene oceanographic variability in Disko Bugt, West Greenland, Quaternary Sci. Rev., 30, 2815–2826, https://doi.org/10.1016/j.quascirev.2011.06.018, 2011.

Perner, K., Moros, M., Lloyd, J. M., Jansen, E., and Stein, R.: Mid to late Holocene strengthening of the East Greenland Current linked to warm subsurface Atlantic water, Quaternary Sci. Rev., 129, 296–307, https://doi.org/10.1016/j.quascirev.2015.10.007, 2015.

Porter, C., Morin, P., Howat, I., Noh, M.-J., Bates, B., Peterman, K., Keesey, S., Schlenk, M., Gardiner, J., Tomko, K., Willis, M., Kelleher, C., Cloutier, M., Husby, E., Foga, S., Nakamura, H., Platson, M., Wethington Jr., M., Williamson, C., Bauer, G., Enos, J., Arnold, G., Kramer, W., Becker, P., Doshi, A., D'Souza, C., Cummens, P., Laurier, F., and Bojesen, M.: ArcticDEM (V1), Harvard Dataverse [data set], https://doi.org/10.7910/DVN/OHHUKH, 2018.

Prahl, F. G. and Wakeham, S. G.: Calibration of unsaturation patterns in long-chain ketone compositions for palaeotemperature assessment, Nature, 330, 367–369, https://doi.org/10.1038/330367a0, 1987.

Prahl, F. G., Muehlhausen, L. A., and Zahnle, D. L.: Further evaluation of long-chain alkenones as indicators of paleoceanographic conditions, Geochim. Cosmochim. Ac., 52, 2303–2310, https://doi.org/10.1016/0016-7037(88)90132-9, 1988.

Rasmussen, S. O., Abbott, P. M., Blunier, T., Bourne, A. J., Brook, E., Buchardt, S. L., Buizert, C., Chappellaz, J., Clausen, H. B., Cook, E., Dahl-Jensen, D., Davies, S. M., Guillevic, M., Kipfstuhl, S., Laepple, T., Seierstad, I. K., Severinghaus, J. P., Steffensen, J. P., Stowasser, C., Svensson, A., Vallelonga, P., Vinther, B. M., Wilhelms, F., and Winstrup, M.: A first chronology for the North Greenland Eemian Ice Drilling (NEEM) ice core, Clim. Past, 9, 2713–2730, https://doi.org/10.5194/cp-9-2713-2013, 2013.

Rasmussen, T. L., Pearce, C., Andresen, K. J., Nielsen, T., and Seidenkrantz, M.-S.: Northeast Greenland: ice-free shelf edge at 79.4° N around the Last Glacial Maximum 25.5–17.5 ka, Boreas, **TS2**, https://doi.org/10.1111/bor.12593, 2022.

Reimer, P. J., Bard, E., Bayliss, A., Beck, J. W., Blackwell, P. G., Ramsey, C. B., Buck, C. E., Cheng, H., Edwards, R. L., Friedrich, M., Grootes, P. M., Guilderson, T. P., Haflidason, H., Hajdas, I., Hatte, C., Heaton, T. J., Hoffmann, D. L., Hogg, A. G., Hughen, K. A., Kaiser, K. F., Kromer, B., Manning, S. W., Niu, M., Reimer, R. W., Richards, D. A., Scott, E. M., Southon, J. R., Staff, R. A., Turney, C. S. M., and van der Plicht, J.: Intcal13 and Marine13 Radiocarbon Age Calibration Curves 0–50,000 Years cal BP, Radiocarbon, 55, 1869–1887, https://doi.org/10.2458/azu_js_rc.55.16947, 2013.

Rieley, G., Collier, R. J., Jones, D. M., Eglinton, G., Eakin, P. A., and Fallick, A. E.: Sources of sedimentary lipids deduced from stable carbon-isotope analyses of individual compounds, Nature, 352, 425–427, https://doi.org/10.1038/352425a0, 1991.

Robel, A. A.: Thinning sea ice weakens buttressing force of iceberg mélange and promotes calving, Nat. Commun., 8, 14596, https://doi.org/10.1038/ncomms14596, 2017.

Rosell-Melé, A. and McClymont, E. L.: Chapter Eleven Biomarkers as Paleoceanographic Proxies, in: Developments in Marine Geology, edited by: Hillaire–Marcel, C. and De Vernal, A., Elsevier, 441–490, https://doi.org/10.1016/S1572-5480(07)01016-0, 2007.

Sánchez-Montes, M. L., McClymont, E. L., Lloyd, J. M., Müller, J., Cowan, E. A., and Zorzi, C.: Late Pliocene Cordilleran Ice Sheet development with warm northeast Pacific sea surface temperatures, Clim. Past, 16, 299–313, https://doi.org/10.5194/cp-16-299-2020, 2020.

Schaffer, J., Kanzow, T., von Appen, W.-J., von Albedyll, L., Arndt, J. E., and Roberts, D. H.: Bathymetry constrains ocean heat supply to Greenland's largest glacier tongue, Nat. Geosci., 13, 227–231, https://doi.org/10.1038/s41561-019-0529-x, 2020.

Seki, A., Tada, R., Kurokawa, S., and Murayama, M.: High-resolution Quaternary record of marine organic carbon content in the hemipelagic sediments of the Japan Sea from bromine counts measured by XRF core scanner, Progress in Earth and Planetary Science, 6, 1, https://doi.org/10.1186/s40645-018-0244-z, 2019.

Seroussi, H., Morlighem, M., Rignot, E., Khazendar, A., Larour, E., and Mouginot, J.: Dependence of century-scale projections of the Greenland ice sheet on its thermal regime, J. Glaciol., 59, 1024–1034, https://doi.org/10.3189/2013JoG13J054, 2013.

Slubowska-Wodengen, M., Rasmussen, T. L., Koc, N., Klitgaard-Kristensen, D., Nilsen, F., and Solheim, A.: Advection of Atlantic Water to the western and northern Svalbard shelf since 17,500 cal yr BP, Quaternary Sci. Rev., 26, 463–478, https://doi.org/10.1016/j.quascirev.2006.09.009, 2007.

Slubowska, M. A., Koc, N., Rasmussen, T. L., and Klitgaard-Kristensen, D.: Changes in the flow of Atlantic water into the Arctic Ocean since the last deglaciation: Evidence from the northern Svalbard continental margin, 80° N, Paleoceanography, 20, Pa4014, https://doi.org/10.1029/2005pa001141, 2005.

Smith, J., Callard, L., Sanchez Montes, M., McClymont, E., Lloyd, J., Ehrmann, W., Roberts, D., Bentley, M., Jamieson, S., Lane, T., and Darvill, C.: Chronological sedimentological data (radiocarbon 14C) for cores LC7 and LC12 sediment record from Blaso, a large, epishelf lake in NW Greenland collected July–August 2017 (Version 1.0), NERC EDS UK Polar Data Centre [data set], https://doi.org/10.5285/e44bbc45-9924-401b-a7b8-7939fbb61db2, 2022.

Smith, J. A., Hodgson, D. A., Bentley, M. J., Verleyen, E., Leng, M. J., and Roberts, S. J.: Limnology of two antarctic epishelf lakes and their potential to record periods of ice shelf loss, J. Paleolimnol., 35, 373–394, https://doi.org/10.1007/s10933-005-1333-8, 2006.

Smith, J. A., Bentley, M. J., Hodgson, D. A., Roberts, S. J., Leng, M. J., Lloyd, J. M., Barrett, M. S., Bryant, C., and Sugden, D. E.: Oceanic and atmospheric forcing of early Holocene ice shelf retreat, George VI Ice Shelf, Antarctica Peninsula, Quaternary Sci. Rev., 26, 500–516, https://doi.org/10.1016/j.quascirev.2006.05.006, 2007.

Smith, M. P., Higgins, A. K., Soper, N. J., and Sønderholm, M.: The Neoproterozoic Rivieradal Group of Kronprins Christian Land, eastern North Greenland, Geol. Surv. Den. Greenl., 6, 29–39, https://doi.org/10.34194/geusb.v6.4816, 2004a.

Smith, M. P., Rasmussen, J. A., Robertson, S., Higgins, A. K., and Leslie, A. G.: Lower Palaeozoic stratigraphy of the East Greenland Caledonides, Geol. Surv. Den. Greenl., 6, 5–28, https://doi.org/10.34194/geusb.v6.4815, 2004b.

Straneo, F. and Heimbach, P.: North Atlantic warming and the retreat of Greenland's outlet glaciers, Nature, 504, 36–43, https://doi.org/10.1038/nature12854, 2013.

Stuiver, M. and Reimer, P. J.: Extended 14C database and revised CALIB 3.0 radiocarbon calibration program, Radiocarbon 35, 215–230, https://doi.org/10.1017/S0033822200013904, 1993.

Syring, N., Lloyd, J. M., Stein, R., Fahl, K., Roberts, D. H., Callard, L., and O'Cofaigh, C.: Holocene Interactions Between Glacier Retreat, Sea Ice Formation, and Atlantic Water Advection at the Inner Northeast Greenland Continental Shelf, Paleoceanography and Paleoclimatology, 35, e2020PA004019, https://doi.org/10.1029/2020PA004019, 2020.

ten Haven, H. L., de Leeuw, J. W., Sinninghe Damsté, J. S., Schenck, P. A., Palmer, S. E., and Zumberge, J. E.: Application of biological markers in the recognition of palaeohypersaline environments, Geological Society, London, Special Publications, 40, 123, https://doi.org/10.1144/GSL.SP.1988.040.01.11, 1988.

Turton, J. V., Hochreuther, P., Reimann, N., and Blau, M. T.: The distribution and evolution of supraglacial lakes on 79° N Glacier (north-eastern Greenland) and interannual climatic controls, The Cryosphere, 15, 3877–3896, https://doi.org/10.5194/tc-15-3877-2021, 2021.

Wagner, B. and Melles, M.: A Holocene seabird record from Raffles Sø sediments, East Greenland, in response to climatic and oceanic changes, Boreas, 30, 228–239, https://doi.org/10.1111/j.1502-3885.2001.tb01224.x, 2001.

Wagner, B., Melles, M., Hahne, J., Niessen, F., and Hubberten, H. W.: Holocene climate history of Geographical Society Ø, East Greenland — evidence from lake sediments, Palaeogeogr. Palaeocl., 160, 45–68, https://doi.org/10.1016/S0031-0182(00)00046-8, 2000.

Walinsky, S. E., Prahl, F. G., Mix, A. C., Finney, B. P., Jaeger, J. M., and Rosen, G. P.: Distribution and composition of organic matter in surface sediments of coastal Southeast Alaska, Cont. Shelf Res., 29, 1565–1579, https://doi.org/10.1016/j.csr.2009.04.006, 2009.

Wang, K. J., Huang, Y., Majaneva, M., Belt, S. T., Liao, S., Novak, J., Kartzinel, T. R., Herbert, T. D., Richter, N., and Cabedo-Sanz, P.: Group 2i Isochrysidales produce characteristic alkenones reflecting sea ice distribution, Nat. Commun., 12, 15, https://doi.org/10.1038/s41467-020-20187-z, 2021.

Werner, K., Müller, J., Husum, K., Spielhagen, R. F., Kandiano, E. S., and Polyak, L.: Holocene sea subsurface and surface water masses in the Fram Strait – Comparisons of temperature and sea-ice reconstructions, Quaternary Sci. Rev., 147, 194–209, https://doi.org/10.1016/j.quascirev.2015.09.007, 2016.

Winkelmann, D., Jokat, W., Jensen, L., and Schenke, H.-W.: Submarine end moraines on the continental shelf off NE Greenland – Implications for Lateglacial dynamics, Quaternary Sci. Rev., 29, 1069–1077, https://doi.org/10.1016/j.quascirev.2010.02.002, 2010.

Winnell, M. H. and White, D. S.: The Distribution of *Heterotrissocladius oliveri* Saether (Diptera: Chironomidae) in Lake Michigan, Hydrobiologia, 131, 205–214, https://doi.org/10.1007/Bf00008856, 1986.

Wollenburg, J. E. and Mackensen, A.: On the vertical distribution of living (Rose Bengal stained) benthic foraminifers in the Arctic Ocean, J. Foramin. Res., 28, 268–285, https://doi.org/10.2113/gsjfr.28.4.268, 1998.

Wood, M., Rignot, E., Fenty, I., An, L., Bjørk, A., van den Broeke, M., Cai, C., Kane, E., Menemenlis, D., Millan, R., Morlighem, M., Mouginot, J., Noël, B., Scheuchl, B., Velicogna, I., Willis, J. K., and Zhang, H.: Ocean forcing drives glacier retreat in Greenland, Science Advances, 7, eaba7282, https://doi.org/10.1126/sciadv.aba7282, 2021.

Yin, J., Overpeck, J. T., Griffies, S. M., Hu, A., Russell, J. L., and Stouffer, R. J.: Different magnitudes of projected subsurface ocean warming around Greenland and Antarctica, Nat. Geosci., 4, 524–528, https://doi.org/10.1038/ngeo1189, 2011.

Ziegler, M., Jilbert, T., de lange, G. J., Lourens, L. J., and Reichart, G.-J.: Bromine counts from XRF scanning as an estimate of the marine organic carbon content of sediment cores, Geochem. Geophy. Geosy., 9, Q05009, https://doi.org/10.1029/2007gc001932, 2008.

Remarks from the language copy-editor

CE1   There are a few options here: (a) keep it as it is; (b) make it italic and end it in a full stop (*LF1*. The...); or (c) make "LF1" a proper subheading.

CE2   Please check the text here: it was unclear which minor edit you were referring to.

CE3   chronological? Please check the spelling.

Remarks from the typesetter

TS1   Please provide DOI or ISBN.

TS2   Please provide the volume number and article number or page range.